

---

# A NONLOCAL MODELING FOR SOLVING TIME FRACTIONAL DIFFUSION EQUATION ARISING IN FLUID MECHANICS

VAHID REZA HOSSEINI,\* AREZOU REZAZADEH,<sup>†</sup>  
HUI ZHENG<sup>‡,§</sup> and WENNAN ZOU\*

\**Institute for Advanced Study  
Nanchang University, P. R. China*

<sup>†</sup>*Department of Mathematics  
University of Qom, Qom 37161466711, Iran*

<sup>‡</sup>*School of Infrastructure Engineering  
Nanchang University, Nanchang, P. R. China*  
§zhenghui@ncu.edu.cn

Received January 15, 2021

Accepted November 10, 2021

Published August 10, 2022

## Abstract

This study mainly investigates new techniques for obtaining numerical solutions of time-fractional diffusion equations. The fractional derivative term is represented in the Lagrange operational sense. First, we describe the temporal direction of the considered model using the Legendre orthogonal polynomials. Moreover, to archive a full discretization approach a type of nonlocal method has been applied that is known as the nonlocal peridynamic differential

---

<sup>§</sup>Corresponding author.

This is an Open Access article in the “Special Issue Section on Fractal AI-Based Analyses and Applications to Complex Systems: Part III”, edited by Yeliz Karaca (University of Massachusetts Medical School, USA), Dumitru Baleanu (Cankaya University, Turkey), Majaz Moonis (University of Massachusetts Medical School, USA), Yu-Dong Zhang (University of Leicester, UK) & Osvaldo Gervasi (Perugia University, Italy) published by World Scientific Publishing Company. It is distributed under the terms of the Creative Commons Attribution 4.0 (CC-BY) License which permits use, distribution and reproduction in any medium, provided the original work is properly cited.

operator (PDDO). The PDDO is based on the concept of peridynamic (PD) interactions by proposing the PD functions orthogonal to each term in the Taylor Series Expansion (TSE) of a field variable. The PDDO for numerical integration uses the vicinity of each point (referred to as the horizon, which does not need background mesh). The PDDO is exclusively described in terms of integration (summation) throughout the interaction domain. As a result, it is unsusceptible to singularities caused by discontinuities. It does, however, need the creation of PD functions at each node. We numerically investigate the stability, the convergence of the scheme, which verifies the validity of the proposed method. Numerical results show the simplicity and accuracy of the presented method.

*Keywords:* Time Fractional Equation; Meshless; Nonlocal Model; Peridynamic Differential Operator.

## 1. INTRODUCTION

Over the past few decades, there has been a perceptible increase in the investigation in fractional diffraction equations (FDEs) theoretically and numerically. Fractional calculus provides a mathematical framework for modeling spatiotemporal systems across the varied phenomena in physics and engineering, e.g. fluid mechanics, vibration, heat and optimization.<sup>1–5</sup> Many real-world physical systems make intelligible dynamics of fractional order and their behaviors are modeled FDEs. All in all, FDEs are arbitrary-order extensions of order differential equations. The reason for the popularity of FDEs is their nonlocal property.<sup>7,8,31</sup> The nonlocal character simply means that the evolution of the solution at current time level of the dynamical processing depends on its solution at previous time level which saved in storage at every time level. Recent efforts have shown that it is possible to apply FPDs to discover advantageous memory processes for dynamical systems.<sup>9–11</sup> Interestingly, such architectures offer a new mathematical framework strategy for modeling spatiotemporal systems across physical and engineering sciences. As a result, one of the key motivations for adopting these derivatives in diverse applications is their memory effect. As a result, FDEs have become popular for characterizing various processes, including those in fluid mechanics, finance, health care, etc.<sup>12–17</sup> It should be emphasized that due to their enormous complexity, solving fractional differential equations analytically is exceedingly difficult, if not impossible in most cases. As a result, in most cases, we must seek numerical solutions for them. Thus, presenting efficient and accurate numerical approaches for finding numerical solutions to these types of

issues is important in practice. Generally speaking, numerous studies have demonstrated the effectiveness of finite-difference methods nowadays popular for approximating numerical solution of FDEs. Although finite difference methods are particularly successful for solving numerous types of FDEs, their usefulness is limited by the conditional stability of explicit finite difference procedures and the necessity for a large amount of processor time in implicit finite difference methods. On the other hand, for particular types of problems, meshing the domain can be complex and time-consuming.

Meshless approaches have received a lot of interest from researchers over the last few decades. As a result, there is an increasing interest in developing meshless approaches that avoid or significantly reduce the problems associated with boundary or domain meshing. Meshless approaches are increasingly being recognized as an effective alternative to mesh-based methods for a certain set of challenges for a certain class of problems including TFDEs.<sup>18</sup>

The nonlocal description of a scalar field at a material location is assessed in terms of its nonlocal interactions with other points, and the intensity of those interactions is characterized by a weight function. This means that peridynamic differential operator (PDDO) employs an integro-differential operator that resembles the integration operator employed in the Peridynamic equation of motion. Instead of using a direct differentiation procedure, this operator can be adopted to approximate a function and its derivatives. The most striking result to emerge from PDDO is that once the horizon approaches zero the operator asymptotically recasts the direct differentiation, in other words, the

peridynamic (PD) differentiation recasts the local differentiation. It transforms differentiation from a local to a nonlocal PD form. In fact, PD form is a link between differentiation and integration. The PDDO allows for numerical differentiation via integration.

Instead of using the shape function based on interpolation approaches, the differential operator on field value is taken into account as the nonlocal interplays between the points in each subdomain. Li<sup>19</sup> developed a nonlocal differential operator under total and updated Lagrangian frameworks, directly inspired by the mathematical statement of the nonlocal equation of motion of state-based PD.<sup>20–23</sup> Instead of using partial differential equations, the nonlocal PD form has been suggested. The proposed method, PD approach, emerged to deal with the presence of jump discontinuities and singularity.<sup>24</sup> Thus, it is no wonder that PD method has been successful in many phenomena in physics and engineering, e.g. crack propagation, laminar fluid motion, etc.<sup>19,25–29</sup> However, the employability of PD approach through partial differential equations PDEs and FPDEs is still in its infant stage. To the best of our knowledge, there is no previous research focused on using PD method for time-fractional partial differential equations (TPFEs) in two dimensions. This motivates our interest to introduce the novel numerical approach for solving TPFEs.

The idea of work on nonlocal differential operator within the spirit Taylor Series Expansion (TSE) and orthogonal function was undertaken by Madenci *et al.*<sup>30</sup> The PD theory does not suffer from implementation material properties.<sup>19,31–33</sup> In addition, the corresponding partial differential equations (PDEs) can be reformulated into their integral term directly. The classical physical parameters without transforming into their PD terms can be exploited directly.<sup>30,34</sup> Hence, the corresponding order derivatives may be evaluated via one integration through utilizing the proposed PD differential. When determining the expressions of the PD differential operators, both lower and higher-order terms are considered.<sup>35–38</sup>

The main objective of this investigation is numerical solution of two-dimensional time fractional convection-diffusion equation. For this purpose, the time-fractional derivative is addressed by means of Lagrange operational matrix. For this purpose, the Legendre orthogonal polynomials are used as base functions for evaluating Caputo derivative. We

generate a set of uniform points in computational spatial domain. We implement PD method for the spatial direction discretization based on TSEs. The given governing equation and its initial and boundary conditions transform corresponding to integral form which leads to solving a linear system of algebraic equation. The two-dimensional time fractional diffusion equation problem is governed by

$$\begin{cases} {}_0^c D_t^\alpha u(\mathbf{x}, t) = \Delta u(\mathbf{x}, t) - \gamma u(\mathbf{x}, t) + f(\mathbf{x}, t), \\ \quad (x, y) \in Q, \quad 0 < t \leq T, \\ u(\mathbf{x}, t) = \rho(\mathbf{x}, t), \quad (x, y) \in \Omega, \\ u(\mathbf{x}, 0) = u_0(\mathbf{x}), \quad (x, y) \in \partial\Omega, \quad 0 < t \leq T, \end{cases} \quad (1)$$

where  $\Omega = [0, 1]^2$  is the spatial domain and  $\partial\Omega$  is the boundary of  $\Omega$ . Let  $Q = \Omega \times (0, 1]$  and  $\Sigma = \partial\Omega \times (0, 1]$ . The functions  $\rho(\mathbf{x}, t)$  and  $u_0(\mathbf{x})$  and the source term  $f(\mathbf{x}, t)$  are given and are assumed sufficiently smooth. Moreover,  $\Delta = \frac{\partial^2}{\partial x^2} + \frac{\partial^2}{\partial y^2}$  denotes the Laplacian differential operator  $\gamma$  which is reaction coefficient and the fractional derivative of Eq. (1) in the Caputo sense is stated as

$${}_0^c D_t^\alpha f(t) = \begin{cases} \frac{1}{\Gamma(n-\alpha)} \int_{t_0}^t (t-\tau)^{n-\alpha-1} \frac{d^n}{d\tau^n} \\ \quad \times f(\tau) d\tau, \quad 0 \leq n-1 < \alpha < n, \\ f^{(n)}(t), \quad \alpha = n, \end{cases} \quad (2)$$

in which  ${}_0^c D_t^\alpha f(t)$  is the Caputo fractional derivative ones of arbitrary order  $0 < \alpha < 1$ . The fractional diffusion equation can be used to address the anomalous diffusion or wave propagation in complex systems because of using a memory effect.<sup>39–41</sup> It seemed inconceivable to investigate diffusion processes through experimental method or even analytical solution due to time-consuming and expensive possesses. To overcome intrinsic limitations of *in vitro* study theoretically, numerical approaches with growing efforts have been described as phenomenal including diffusion mechanism. Up to now, numerous numerical schemes to explain the diffusion mechanism have been proposed. Lin *et al.*<sup>42</sup> carried out Finite difference/spectral approximations in the time-fractional diffusion. In space-time spectral scheme has been applied via introducing the concept of a well-suited variational formulation by Ref. 10. The Grünwald–Letnikov discretization of the Riemann–Liouville sense based on the high-order compact

finite difference has been proposed in Ref. 43. In Ref. 44, Hosseini *et al.* developed a proposed meshless method for spatial discretization and finite difference method for the time direction and proved that the scheme was unconditionally stable. Alikhanov in Ref. 45 formulated the Caputo fractional via new difference which has a significant role and is time-consuming. The unconditional stability and convergence of the in the framework of second-order difference scheme is present. As is reported in Ref. 46, the shortage of smoothness of the solution in  $t = 0$  leads to singularity. To tackle this drawback, Stynes and coworkers established a new approach to deal with uniform and nonuniform mesh distribution. The following assumption will be deferred until Sec. 3.

**Definition 1.** Consider  $C = (c_{ij})_{m \times n}$  and  $D$  are two arbitrary matrices. Kroncker product of  $C$  and  $D$  is defined as

$$C \otimes D = \begin{bmatrix} c_{11}D & c_{12}D & \cdots & c_{1n}D \\ c_{21}D & c_{22}D & \cdots & c_{2n}D \\ \vdots & \vdots & \ddots & \vdots \\ c_{m1}D & c_{m2}D & \cdots & c_{mn}D \end{bmatrix}.$$

**Definition 2.** Assume  $C = (c_{ij})_{m \times n}$  to be a given matrix, then  $\text{vec}(C)$  is a column vector made of the column of  $C$  stacked a top one another from left to right that the size of it is  $m \times n$ .

$$\text{vec}(C) = (c_{11}, c_{21}, \dots, c_{m1}, c_{12}, c_{22}, \dots, c_{m2}, \dots, c_{1n}, \dots, c_{mn})^T.$$

We refer the reader to Ref. 47. The content will be organized as follows. In the following section, the concept of PDDO and the properties of Legendre polynomials are concisely introduced. Section 3 is devoted to implementing Legendre polynomials in the fractional term and the resulting equation is evaluated numerically via the proposal meshless scheme in two dimensions. In Sec. 4, several numerical experiments illustrate the effectiveness and accuracy of the proposed technique. Eventually, a short conclusion is drawn in Sec. 5.

## 2. NUMERICAL SCHEME

The numerical scheme discussed in this study is comprised of two major components: a PDOD capable of working with uniform and non-uniform scattering points and later, we present Shifted Legendre polynomials as the base of the approximate the of the Caputo derivative.

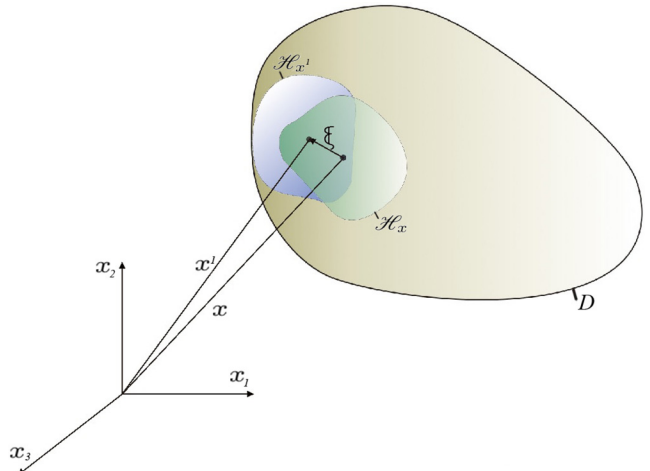


**Fig. 1** Interaction of PD points  $x$  and  $x'$  with arbitrary family size and shape.

### 2.1. Peridynamic Differential Concept

To understand any method, it is always helpful to understand the problem it was created to solve, the history can make it obvious what advantages and disadvantages a method has. In the following section, we introduce PDOD to understand the conception of the PDOD. The first serious discussion and analyses of PD theory emerged during the 2000s with Silling.<sup>48</sup> As demonstrated in Fig. 1, the computational domain discretized without implementation of the predefined mesh, it means that any set of nodes scattered in computational domain and on the boundaries can be used. Every PD node has associated with the vicinity nodes whose distance is less than  $\delta$ . Hence,  $\mathbf{x}$  denotes the coordinate of the node of interest (source point) and the  $\mathbf{x}'$  are so-called family members. The local domain in which  $\mathbf{x}$  interacts with family members was introduced in the horizon. Radius  $\delta$  represents measure of nonlocal effects (horizon length). The vector of  $\xi$  determines initial relative position between  $\mathbf{x}$  and  $\mathbf{x}'$ , i.e.  $\xi = \mathbf{x} - \mathbf{x}'$ . It is noted that depending on location of node of interest,  $\mathbf{x}$ , unique family members have difference in terms of position, shape and size that remarkably have impacted on the degree of nonlocality. In each family, the degree of the interaction between the nodes is presented in the weight function. It emphasizes the nondimensional weight function,  $w(|\xi|)$ , which might be different from node to node. Family size and shape play a crucial role in determining interactions, in other words, reducing family size leads to most local interactions.<sup>49–51</sup>

## 2.2. Peridynamic Differential Concept

In this subsection, let us consider two-dimensional space, the TSE of a scalar field  $f(\mathbf{x}') = f(\mathbf{x} + \xi)$  with respect  $\mathbf{x} := (x, y) = (x_1, x_2)$  as

$$f(\mathbf{x} + \xi) = \sum_{n_1=0}^N \sum_{n_2=0}^{N-n_1} \frac{1}{n_1! n_2!} \xi_1^{n_1} \xi_2^{n_2} \frac{\partial^{n_1+n_2} f(\mathbf{x})}{\partial x_1^{n_1} \partial x_2^{n_2}} + R(N, \mathbf{x}) \quad 0 < n_1 + n_2 \leq 2. \quad (3)$$

In what follows,  $n_1$  and  $n_2$  denote the differential order with respect to  $x$  and  $y$ . Here,  $R(N, \mathbf{x})$  represents the remainder and we use notation  $\xi = \mathbf{x} - \mathbf{x}'$  in which  $\mathbf{x}$  accounts for the effect of its interactions with the other points,  $\mathbf{x}'$ , in the domain. The small term  $R(N, \mathbf{x})$  may be neglected, we can express the above equation for  $n_{x_1}, n_{x_2} = 0, 1, 2$  as follows:

$$\begin{aligned} f(\mathbf{x} + \xi) = f(\mathbf{x}) &+ \xi_1 \frac{\partial f(\mathbf{x})}{\partial x_1} + \xi_2 \frac{\partial f(\mathbf{x})}{\partial x_2} \\ &+ \frac{1}{2} \xi_1^2 \frac{\partial^2 f(\mathbf{x})}{\partial x_1^2} + \frac{1}{2} \xi_2^2 \frac{\partial^2 f(\mathbf{x})}{\partial x_2^2} \\ &+ \xi_1 \xi_2 \frac{\partial^2 f(\mathbf{x})}{\partial x_1 \partial x_2}. \end{aligned} \quad (4)$$

In general, the PDDO is defined by

$$g_N(\xi)^{p_1 p_2} \triangleq \frac{\partial^{p_1+p_2} f(x)}{\partial x_1^{p_1} \partial x_2^{p_2}}, \quad 0 < n_1 + n_2 \leq 2. \quad (5)$$

Taking Eq. (4), by multiplying  $g_N^{p_1 p_2}(\xi)$  and integrating over sub-domain related to own family member, we obtain

$$\begin{aligned} &\int_{\mathcal{H}_x} f(\mathbf{x} + \xi) g_N^{p_1 p_2}(\xi) d\mathcal{V} \\ &= f(\mathbf{x}) \int_{\mathcal{H}_x} g_N^{p_1 p_2}(\xi) d\mathcal{V} \\ &+ \frac{\partial f(\mathbf{x})}{\partial x_1} \int_{\mathcal{H}_x} \xi_1 g_N^{p_1 p_2}(\xi) d\mathcal{V} \\ &+ \frac{\partial f(\mathbf{x})}{\partial x_2} \int_{\mathcal{H}_x} \xi_2 g_N^{p_1 p_2}(\xi) d\mathcal{V} \\ &+ \frac{1}{2} \frac{\partial^2 f(\mathbf{x})}{\partial x_1^2} \int_{\mathcal{H}_x} \xi_1^2 g_N^{p_1 p_2}(\xi) d\mathcal{V} \\ &+ \frac{1}{2} \frac{\partial^2 f(\mathbf{x})}{\partial x_2^2} \int_{\mathcal{H}_x} \xi_2^2 g_N^{p_1 p_2}(\xi) d\mathcal{V} \\ &+ \frac{\partial^2 f(\mathbf{x})}{\partial x_1 \partial x_2} \int_{\mathcal{H}_x} \xi_1 \xi_2 g_N^{p_1 p_2}(\xi) d\mathcal{V}. \end{aligned} \quad (6)$$

To demonstrate the performance of PD scheme for the two-dimensional, we consider Eq. (6) to obtain the following relation:

$$\begin{aligned} &\int_{\mathcal{H}_x} (f(\mathbf{x} + \xi) - f(\mathbf{x})) g_N(\xi)^{p_1 p_2} d\mathcal{V} \\ &= \sum_{n_1=0}^2 \sum_{n_2=0}^{2-n_1} \frac{1}{n_1! n_2!} \int_{\mathcal{H}_x} \frac{\partial^{n_1+n_2} f(\mathbf{x})}{\partial x_1^{n_1} \partial x_2^{n_2}} \\ &\quad \times \xi_1 \xi_2 g_N(\xi)^{p_1 p_2} d\mathcal{V}. \end{aligned}$$

To impose orthogonality feature, the partial derivatives of various order derivatives PD are described as follows:

$$\begin{aligned} &\int_{\mathcal{H}_x} f(\mathbf{x} + \xi) g_N(\xi)^{p_1 p_2} dx_1 dx_2 \\ &= \frac{1}{p_1! p_2!} \int_{\mathcal{H}_x} \frac{\partial^{n_1+n_2} f(\mathbf{x})}{\partial x_1^{n_1} \partial x_2^{n_2}} \xi_{x_1} \xi_{x_2} g_N(\xi)^{p_1 p_2} d\mathcal{V} \\ &= \frac{\partial^{p_1+p_2} f(\mathbf{x})}{\partial x_1^{p_1} \partial x_2^{p_2}}, \end{aligned} \quad (7)$$

where  $p_i$  stands for the order of differentiation with respect to  $x_i$  with  $i = 1, 2$ .<sup>49</sup>

$$\left[ \begin{array}{c} f(\mathbf{x}) \\ \frac{\partial f(\mathbf{x})}{\partial x_1} \\ \frac{\partial f(\mathbf{x})}{\partial x_2} \\ \frac{\partial^2 f(\mathbf{x})}{\partial x_1^2} \\ \frac{\partial^2 f(\mathbf{x})}{\partial x_2^2} \\ \frac{\partial^2 f(\mathbf{x})}{\partial x_1 \partial x_2} \end{array} \right] = \int_{\mathcal{H}_x} f(\mathbf{x} + \xi) \left[ \begin{array}{c} g_2^{00}(\xi) \\ g_2^{10}(\xi) \\ g_2^{01}(\xi) \\ g_2^{20}(\xi) \\ g_2^{02}(\xi) \\ g_2^{11}(\xi) \end{array} \right] d\mathcal{V}. \quad (8)$$

The operator PD  $g_N^{p_1 p_2}(\xi)$  represents the desired the  $\delta$ -Kronecker properties. Hence, we achieve the following relation as

$$\frac{1}{n_1! n_2!} \int_{\mathcal{H}_x} \xi_1^{n_1} \xi_2^{n_2} g_N^{p_1 p_2}(\xi) dx_1 dx_2 = \delta_{n_1 p_1} \delta_{n_2 p_2}, \quad (9)$$

in which  $n_1 p_1$  and  $n_2 p_2$  indicates !!and  $g_N^{p_1 p_2}$  is known as function and can be constructed as

$$g_N^{p_1 p_2}(\xi) = \sum_{q_1=0}^N \sum_{q_2=0}^{N-q_1} a_{q_1 q_2}^{p_1 p_2} w_{q_1 q_2}(|\xi|) \xi_1^{q_1} \xi_2^{q_2}, \quad (10)$$

where  $w_{q_1 q_2}(|\xi|)$  is the weight function due to the nature of the nonlocality which can be various for

each term in the  $\xi_1^{q_1} \xi_2^{q_2}$ . To find numerical approximation, we should determine the  $a_{q_1 q_2}^{p_1 p_2}$  coefficients:

$$\sum_{q_1=0}^N \sum_{q_2=0}^{N-q_1} A_{(n_1 n_2)(q_1 q_2)} a_{q_1 q_2}^{p_1 p_2} = b_{n_1 n_2}^{p_1 p_2}, \quad (11)$$

in which  $q_i = 0, \dots, N$ . The matrix  $A_{(n_1 n_2)(q_1 q_2)}$  can be written in the following form:

$$A_{(n_1 n_2)(q_1 q_2)} = \int_{\mathcal{H}_x} w_{q_1 q_2}(\xi) \xi_1^{n_1+q_1} \xi_2^{n_2+q_2} d\nu, \quad (12)$$

and

$$b_{n_1 n_2}^{p_1 p_2} = n_1! n_2! \delta_{n_1 p_1} \delta_{n_2 p_2}. \quad (13)$$

In accordance with Eq. (10), the PD functions can be expressed in the following form:

$$\begin{aligned} g_2^{p_1 p_2}(\xi) &= a_{00}^{p_1 p_2} w_{00}(|\xi|) + a_{10}^{p_1 p_2} w_{10}(|\xi|) \xi_1 \\ &\quad + a_{01}^{p_1 p_2} w_{01}(|\xi|) \xi_2 + a_{20}^{p_1 p_2} w_{20}(|\xi|) \xi_1^2 \\ &\quad + a_{02}^{p_1 p_2} w_{02}(|\xi|) \xi_2^2 + a_{11}^{p_1 p_2} w_{11}(|\xi|) \xi_1 \xi_2. \end{aligned} \quad (14)$$

Let the weight function be arbitrary. However, for convenience, we provided  $w_{p_1 p_2}(|\xi|) = w(|\xi|)$ . Hence, we can reconstruct Eq. (7) as matrix form as follows:

$$\mathcal{A}\mathbf{a} = \mathbf{b}, \quad (15)$$

where  $\mathcal{A}$  denotes the PD matrix form and the matrix  $\mathbf{a}$  are undetermined coefficients and using Eq. (9) the matrix  $b$  can be considered as following:

$$\begin{aligned} \mathcal{A} &= \int_{\mathcal{H}_x} w(\|\xi\|) \\ &\times \begin{bmatrix} 1 & \xi_1 & \xi_2 & \xi_1^2 & \xi_2^2 & \xi_1 \xi_2 \\ \xi_1 & \xi_1^2 & \xi_1 \xi_2 & \xi_1^3 & \xi_1 \xi_2^2 & \xi_1^2 \xi_2 \\ \xi_2 & \xi_1 \xi_2 & \xi_2^2 & \xi_1^2 \xi_2 & \xi_2^3 & \xi_1 \xi_2^2 \\ \xi_1^2 & \xi_1^3 & \xi_1^2 \xi_2 & \xi_1^4 & \xi_1^2 \xi_2^2 & \xi_1^3 \xi_2 \\ \xi_2^2 & \xi_1 \xi_2^2 & \xi_2^3 & \xi_1^2 \xi_2^2 & \xi_2^4 & \xi_1 \xi_2^3 \\ \xi_1 \xi_2 & \xi_1^2 \xi_2 & \xi_1^2 \xi_2 & \xi_1^3 \xi_2 & \xi_1 \xi_2^3 & \xi_1^2 \xi_2^2 \end{bmatrix} d\nu \end{aligned} \quad (16)$$

and

$$\mathbf{a} = \begin{bmatrix} a_{00}^{00} & a_{00}^{10} & a_{00}^{01} & a_{00}^{20} & a_{00}^{02} & a_{00}^{11} \\ a_{10}^{00} & a_{10}^{10} & a_{10}^{01} & a_{10}^{20} & a_{10}^{02} & a_{10}^{11} \\ a_{01}^{00} & a_{01}^{10} & a_{01}^{01} & a_{01}^{20} & a_{01}^{02} & a_{01}^{11} \\ a_{20}^{00} & a_{20}^{10} & a_{20}^{01} & a_{20}^{20} & a_{20}^{02} & a_{20}^{11} \\ a_{02}^{00} & a_{02}^{10} & a_{02}^{01} & a_{02}^{20} & a_{02}^{02} & a_{02}^{11} \\ a_{11}^{00} & a_{11}^{10} & a_{11}^{01} & a_{11}^{20} & a_{11}^{02} & a_{11}^{11} \end{bmatrix} \quad (17)$$

and

$$\mathbf{b} = \begin{bmatrix} 1 & 0 & 0 & 0 & 0 & 0 \\ 0 & 1 & 0 & 0 & 0 & 0 \\ 0 & 0 & 1 & 0 & 0 & 0 \\ 0 & 0 & 0 & 2 & 0 & 0 \\ 0 & 0 & 0 & 0 & 2 & 0 \\ 0 & 0 & 0 & 0 & 0 & 1 \end{bmatrix}. \quad (18)$$

Coefficients  $\mathbf{a}$  in Eq. (11) can be determined by enforcing Eq. (15) to satisfy the nodes. After solving the linear algebraic system Eq. (15). Substituting coefficients  $\mathbf{a}$  into Eq. (11) leads to approximation solution.

### 2.3. Shifted Legendre Polynomials as Basis of the Approximate the Time Variable

In this section, we represent a scheme to deal with time-fractional term. Instead of discretization via finite difference method to approximate fractional term. The shifted Legendre polynomials of degree  $i+1$  on interval  $[0, 1]$  may be obtained from the recurrence formula as following<sup>47</sup>:

$$\begin{aligned} p'_{i+1}(t) &= \frac{(2i+1)(2t-1)}{(i+1)} p'_i(t) \\ &\quad - \frac{i}{i+1} p'_{i-1}(t), \quad i = 1, 2, 3, \dots, \end{aligned}$$

with  $p'_0(t) = 1$  and  $p'_1(t) = 2t-1$ .

We can define  $p_i(t) = \sqrt{2i+1} p'_i(t)$ . The shifted Legendre polynomials the following orthogonality property is satisfied:

$$\int_0^1 p_i(t) p_j(t) dt = \delta_{ij}. \quad (19)$$

The explicit analytic form of  $p_i(t)$  can be rewritten as

$$p_i(t) = \sqrt{2i+1} \sum_{k=0}^i (-1)^{i+k} \frac{(i+k)! t^k}{(i-k)!(k!)^2}. \quad (20)$$

Assume  $u(t) \in L^2_{\omega_L}[0, 1]$  is developed by means of the shifted Legendre polynomials as the below formula

$$u(t) = \sum_{i=0}^M c_i p_i(t) = \mathbf{C} \Phi(t), \quad (21)$$

Here,  $\Phi(t) = [p_0(t), p_1(t), \dots, p_m(t)]^T$  denotes the shifted Legendre and  $\mathbf{C} = [c_0, c_1, \dots, c_m]$  are coefficients of the corresponding vector  $\Phi(t)$  whose the

components values' entries are determined by the following integration:

$$c_i = \frac{2m+1}{l} \int_0^l u(t)p_i(t)\omega_L dt, \quad i = 0, 1, \dots, m. \quad (22)$$

Furthermore, Legendre polynomials  $\Phi(t)$  can be rewritten in a matrix form as follows:

$$\Phi(t) = \mathbb{A}T_m(t), \quad (23)$$

where

$$\mathbb{A} = \begin{bmatrix} 1 & 0 \\ -\sqrt{3} & 2\sqrt{3} \\ \vdots & \vdots \\ (-1)^m \sqrt{2m+1} & (-1)^{m+1} \sqrt{2m+1} \frac{(m+1)!}{(m-1)!} \\ \cdots & 0 \\ \cdots & 0 \\ \ddots & \vdots \\ \cdots & (-1)^{2m} \sqrt{2m+1} \frac{(2m)!}{(m!)^2} \end{bmatrix},$$

and

$$T_m(t) = [1, t, t^2, \dots, t^m]^T.$$

Subsequently,

$$T_m = \mathbb{A}^{-1} \Phi(t). \quad (24)$$

**Theorem 3 (Refs. 47 and 52).** Assume  $\mathbb{H}$  denotes an inner product space and  $\mathbb{Y} \subset \mathbb{H}$  a complete subspace. Suppose that  $\{\mathbf{e}_0, \mathbf{e}_1, \dots, \mathbf{e}_n\}$  presents a set of an orthogonal basis for  $\mathbb{H}$ . Then, for arbitrary  $\mathbf{f} \in \mathbb{H}$  the best approximation  $\mathbf{f}_0$  of  $f$  in  $\mathbb{Y}$  can be expressed as the following form:

$$\mathbf{f}_0 = \sum_{i=0}^n \langle \mathbf{f}, \mathbf{e}_i \rangle \mathbf{e}_i,$$

such that

$$\forall y \in Y \quad \|\mathbf{f} - \mathbf{f}_0\|_2 \leq \|\mathbf{f} - \mathbb{Y}\|_2,$$

where  $\|\mathbf{f}\|_2 = \sqrt{\langle \mathbf{f}, \mathbf{f} \rangle}$ .

So, we can evaluated  $\mathbf{f}$  as follows:

$$\mathbf{f}(t) \simeq \sum_{j=0}^m c_j p_j(t) = C^T \Phi(t), \quad (25)$$

where  $c_j$  can be determined by following relation:

$$c_j = \langle \mathbf{f}(t), p_j(t) \rangle, \quad (26)$$

and we have

$$C^T = [c_0, \dots, c_m], \quad \Phi^T = [p_0, \dots, p_m]. \quad (27)$$

The operational matrix of the fractional Caputo derivative is constructed which basis on  $\Phi$  the following matrix form can be indicated:

$$D = \begin{bmatrix} D_{11} & D_{12} & \cdots & D_{1(m+1)} \\ \vdots & \vdots & \ddots & \vdots \\ D_{(m+1)1} & D_{(m+1)2} & \cdots & D_{(m+1)(m+1)} \end{bmatrix},$$

where

$$\begin{aligned} \widehat{B}_{i-1j-1} &= \sqrt{(2i+1)(2j+1)} \\ &\times \sum_{k=[\alpha]}^i \sum_{l=0}^j \frac{(-1)^{i+k+j+l} (i+k)!(j+l)!}{(i-k)!k!\Gamma(k+1-\alpha)(j-l)!} \\ &\times (l!)^2 (l+k-\alpha+1) \end{aligned} \quad (28)$$

and

$$D_{ij} = \widehat{B}_{i-1j-1}, \quad 1 \leq i, \quad j \leq m+1.$$

For more details we refer the reader to Refs. 47 and 52.

### 3. DISCRETIZATION USING PERIDYNAMIC METHOD

To discretize spatial term as the intended problem, appearing in Eq. (1), the PD approach is used. In the first step, the domain is directly discretized at the field nodes using the simple collocation techniques. It is worth mentioning that node distribution can be uniform or nonuniform on computational domain and its boundaries. The numerical integration evaluates the performance of PD differential operator Eq. (7). To calculate the integral in regular geometry with uniform distribution for interior nodes, spatial derivatives integration transformed to summation within all family members. Needless to say, in this case, nodes are devoted symmetric family members otherwise the nodes closing the boundaries have symmetric families. One also should not overlook the fact the family size, the property of distributions nodes and weight function have an effect on these functions. In accordance with Eq. (8), the PD differentiation

of a function,  $f(x)$ , is obtained as

$$\frac{d^p f(x)}{dx^p} = \int_{\mathcal{H}_x} f(x + \xi) g_N^p(\xi) d\xi, \quad (29)$$

where  $p$  denotes the order of differentiation and  $N$  represents the number of terms retained in the TSE, in which  $g_N^p(\xi)$  are polynomials' expansion, which can be change depending on the location of nodes. So far, we convert PD differential operator to numerical integration on each family member as follows:

$$\frac{d^p f(x_k)}{dx^p} = \sum_{j=1}^{N_k} f(x_j) g_N^p(x_j - x_k) \mathcal{V}_j, \quad (30)$$

where  $N_k$  is the number of members in the family domain and  $x_j$  denotes the members. Here,  $\mathcal{V}_j$  stands for the small incremental entity of each PD point,  $x_j$ . Thus, finding family members is very important here. We solve the test problems on domain  $[0, 1]^2$  with uniform mesh, as shown in Fig. 2. According to Eq. (30) each function and its derivatives are uniquely associated with size and location of each family. The horizon size of the family can be measured as  $\delta = m\Delta x$  where  $m$  is positive constant integer and  $\Delta x$  indicates the distance between two consecutive nodes in the uniform distribution on the domain. The number of terms,  $N$ , retained in the TSE is dictated by the highest order of differentiation. Also, the number of family members is dependent on  $N$ .

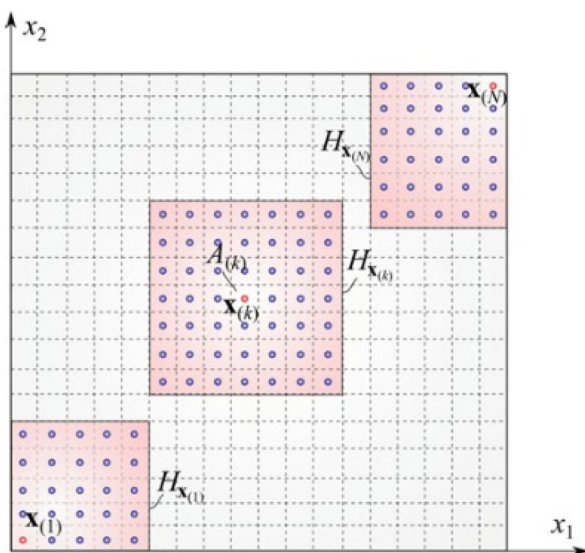


**Fig. 2** The PD discretization of the space-time domain and the description of family.

### 3.1. Discrete of Time-Fractional Diffusion Equation

Employing the PD functions, Eq. (48) is converted to a system of algebraic equations in terms of the PD unknowns,  $u(x_j, t)$  as

$$\begin{aligned} & \sum_{j=1}^{N_k} D_t^\alpha u(\mathbf{x}_{(j)}, t) g_N^{00}(\xi_{1(k)(j)}, \xi_{2(k)(j)}) \mathcal{V}_j \\ & + \sum_{j=1}^{N_k} u(\mathbf{x}_{(j)}, t) (g_N^{20}(\xi_{1(k)(j)}, \xi_{2(k)(j)}) \\ & + g_N^{02}(\xi_{1(k)(j)}, \xi_{2(k)(j)}) \mathcal{V}_j \\ & + \lambda \sum_{j=1}^{N_k} u(\mathbf{x}_{(j)}, t) g_N^{00}(\xi_{1(k)(j)}, \xi_{2(k)(j)}) \mathcal{V}_j \\ & = f(\mathbf{x}_{(k)}, t). \end{aligned} \quad (31)$$

Here and subsequently,  $\xi_{1(k)(j)} = x_{1(j)} - x_{1(k)}$ ,  $\xi_{2(k)(j)} = x_{2(j)} - x_{2(k)}$ ,  $\mathcal{V}_j = \Delta x_1 \Delta x_2$  with uniform spacing of  $\Delta x_1 = \Delta x_2$ . To impose the local boundary and initial conditions, we have

$$\begin{aligned} & \sum_{j=1}^{N_k} u(\mathbf{x}_{(j)}, t) g_N^{00}(\xi_{1(k)(j)}, \xi_{2(k)(j)}) \mathcal{V}_j \\ & = \rho(x_{1(k)}, x_{2(k)}, t), \quad x_{1(k)} = 0 + \frac{\Delta x_1}{2}, \\ & \sum_{j=1}^{N_k} u(\mathbf{x}_{(j)}, t) g_N^{00}(\xi_{1(k)(j)}, \xi_{2(k)(j)}) \mathcal{V}_j \\ & = \rho(x_{1(k)}, x_{2(k)}, t), \quad x_{1(k)} = 1 - \frac{\Delta x_1}{2}, \\ & \sum_{j=1}^{N_k} u(\mathbf{x}_{(j)}, t) g_N^{00}(\xi_{1(k)(j)}, \xi_{2(k)(j)}) \mathcal{V}_j \\ & = \rho(x_{1(k)}, x_{2(k)}, t), \quad x_{2(k)} = 0 + \frac{\Delta x_2}{2}, \\ & \sum_{j=1}^{N_k} u(\mathbf{x}_{(j)}, t) g_N^{00}(\xi_{1(k)(j)}, \xi_{2(k)(j)}) \mathcal{V}_j \\ & = \rho(x_{1(k)}, x_{2(k)}, t), \quad x_{2(k)} = 1 - \frac{\Delta x_2}{2}, \\ & \sum_{j=1}^{N_k} u(\mathbf{x}_{(j)}, t_0) g_N^{00}(\xi_{1(k)(j)}, \xi_{2(k)(j)}) \mathcal{V}_j \\ & = u_0(x_{1(k)}, x_{2(k)}), \end{aligned} \quad (32)$$

in which  $\xi_{1(k)(j)} = x_{1(j)} - x_{1(k)}$ ,  $\xi_{2(k)(j)} = x_{2(j)} - x_{2(k)}$  and  $\mathcal{V}_j$  are expressible as the area of each PD point. We can derive the matrix form of zero derivative

and Laplace operator of  $u$  as  $\mathcal{B}$ ,  $\mathcal{C}$ , respectively. Then using Eq. (30)

$$\begin{bmatrix} \frac{\partial^{0+0} u(\mathbf{x}_1)}{\partial x_1^0 \partial x_2^0} \\ \frac{\partial^{0+0} u(\mathbf{x}_2)}{\partial x_1^0 \partial x_2^0} \\ \vdots \\ \frac{\partial^{0+0} u(\mathbf{x}_M)}{\partial x_1^0 \partial x_2^0} \end{bmatrix} = \mathcal{B} \begin{bmatrix} u(\mathbf{x}_1) \\ u(\mathbf{x}_2) \\ \vdots \\ u(\mathbf{x}_M) \end{bmatrix}, \quad (33)$$

$$\begin{bmatrix} \Delta u(\mathbf{x}_1) \\ \Delta u(\mathbf{x}_2) \\ \vdots \\ \Delta u(\mathbf{x}_M) \end{bmatrix} = \mathcal{C} \begin{bmatrix} u(\mathbf{x}_1) \\ u(\mathbf{x}_2) \\ \vdots \\ u(\mathbf{x}_M) \end{bmatrix}, \quad (34)$$

where  $M$  is the number of points in the domain  $\Omega$ . The nodes divide the matrices  $\mathcal{B}$  and  $\mathcal{C}$  into two parts for interior nodes and boundary points as

$$B = \begin{bmatrix} \mathcal{B}_{\text{int}} \\ \vdots \\ \mathcal{B}_{\text{bound}} \end{bmatrix} \quad C = \begin{bmatrix} \mathcal{C}_{\text{int}} \\ \vdots \\ \mathcal{C}_{\text{bound}} \end{bmatrix}$$

in which subscripts int and bound referred to the rows for the interior points and the boundary points, respectively. Suppose  $n_i$  is the number of points for the interior points and  $n_b$  in the number of points for the boundary points. Then the matrix form of Eq. (33) is as following:

$$\mathcal{B}_{\text{int}} \begin{bmatrix} {}_0^c D_t^\alpha u(\mathbf{x}_1, t) \\ {}_0^c D_t^\alpha u(\mathbf{x}_2, t) \\ \vdots \\ {}_0^c D_t^\alpha u(\mathbf{x}_M, t) \end{bmatrix} - \mathcal{C}_{\text{int}} \begin{bmatrix} u(\mathbf{x}_1, t) \\ u(\mathbf{x}_2, t) \\ \vdots \\ u(\mathbf{x}_M, t) \end{bmatrix} \quad (35)$$

$$+ \lambda \mathcal{B}_{\text{int}} \begin{bmatrix} u(\mathbf{x}_1, t) \\ u(\mathbf{x}_2, t) \\ \vdots \\ u(\mathbf{x}_M, t) \end{bmatrix} = \begin{bmatrix} f(\mathbf{x}_1) \\ f(\mathbf{x}_2) \\ \vdots \\ f(\mathbf{x}_{n_i}) \end{bmatrix}. \quad (36)$$

The boundary conditions is

$$\mathcal{B}_{\text{bound}} \begin{bmatrix} u(\mathbf{x}_1, t) \\ u(\mathbf{x}_2, t) \\ \vdots \\ u(\mathbf{x}_M, t) \end{bmatrix} = \begin{bmatrix} \rho(\mathbf{x}_1, t) \\ \rho(\mathbf{x}_2, t) \\ \vdots \\ \rho(\mathbf{x}_{n_b}, t) \end{bmatrix}, \quad (37)$$

and also the initial conditions is as following:

$$\mathcal{B} \begin{bmatrix} u(\mathbf{x}_1, t_0) \\ u(\mathbf{x}_2, t_0) \\ \vdots \\ u(\mathbf{x}_M, t_0) \end{bmatrix} = \begin{bmatrix} u_0(\mathbf{x}_1) \\ u_0(\mathbf{x}_2) \\ \vdots \\ u_0(\mathbf{x}_M) \end{bmatrix}. \quad (38)$$

To approximate  $u(\mathbf{x}_i, t)$  via Legendre polynomials, time domain can be divided the into  $m$  subintervals where  $t_k = k\delta t$ ,  $k = 0, 1, \dots, m$  and  $\delta t = \frac{1}{m}$ ,

$$u(\mathbf{x}_j, t) = \sum_{i=0}^M u_i^j p_i(t) = [u_0^j, u_1^j, \dots, u_m^j], \quad (39)$$

$$\Phi(t) = u^j \Phi(t),$$

and

$${}_0^c D_t^\alpha u(\mathbf{x}_j, t) = [u_0^j, u_1^j, \dots, u_m^j]; \quad (40)$$

$$D^\alpha \Phi(t) = u^j D^\alpha \Phi(t). \quad (41)$$

We define

$$E = \begin{bmatrix} \mathcal{B}_{\text{int}} \otimes (D^\alpha P)^T - \mathcal{C}_{\text{int}} \otimes P^T - \lambda \mathcal{B}_{\text{int}} \otimes P^T \\ \vdots \\ \mathcal{B}_{\text{bound}} \otimes P^T \\ \vdots \\ \mathcal{B} \otimes P_0^T \end{bmatrix},$$

$$F = \begin{bmatrix} f_{\text{int}} \\ \vdots \\ f_{\text{bound}} \\ \vdots \\ U_0 \end{bmatrix}, \quad (42)$$

where  $P$  and  $P_0$  are the values of the Legendre at points  $t_k$  and  $t_0$ , respectively. The boundary conditions are

$$\mathcal{B}_{\text{bound}} \begin{bmatrix} u(\mathbf{x}_1, t) \\ u(\mathbf{x}_2, t) \\ \vdots \\ u(\mathbf{x}_M, t) \end{bmatrix} = \begin{bmatrix} \rho(\mathbf{x}_1, t) \\ \rho(\mathbf{x}_2, t) \\ \vdots \\ \rho(\mathbf{x}_{n_b}, t) \end{bmatrix}, \quad (43)$$

and the initial conditions are as follows:

$$\mathcal{B} \begin{bmatrix} u(\mathbf{x}_1, t_0) \\ u(\mathbf{x}_2, t_0) \\ \vdots \\ u(\mathbf{x}_M, t_0) \end{bmatrix} = \begin{bmatrix} u_0(\mathbf{x}_1) \\ u_0(\mathbf{x}_2) \\ \vdots \\ u_0(\mathbf{x}_M) \end{bmatrix}. \quad (44)$$

$$P = \begin{bmatrix} p_0(t_1) & p_0(t_2) & \cdots & p_0(t_m) \\ p_1(t_1) & p_1(t_2) & \cdots & p_1(t_m) \\ \vdots & \vdots & \ddots & \vdots \\ p_m(t_1) & p_m(t_2) & \cdots & p_m(t_m) \end{bmatrix}, \quad (45)$$

$$P_0 = \begin{bmatrix} p_0(t_0) \\ p_1(t_0) \\ \vdots \\ p_m(t_0) \end{bmatrix},$$

and

$$\begin{aligned} \mathbf{U}_0 &= [u_0(\mathbf{x}_1), u_0(\mathbf{x}_2), \dots, u_0(\mathbf{x}_M)]^T, \\ \text{vec}(\mathbf{U}) &= [u_0^1, \dots, u_m^1, u_0^2, \dots, u_m^2, \dots, \\ &\quad u_0^M, \dots, u_m^M]^T, \\ \mathbf{f}_{\text{int}} &= [f(\mathbf{x}_1, t_1), \dots, f(\mathbf{x}_{ni}, t_1), f(\mathbf{x}_1, t_2), \dots, \\ &\quad f(\mathbf{x}_{ni}, t_2), f(\mathbf{x}_1, t_m), \dots, f(\mathbf{x}_{ni}, t_m)]^T, \\ \mathbf{f}_{\text{bound}} &= [f(\mathbf{x}_1, t_1), \dots, f(\mathbf{x}_{nb}, t_1), f(\mathbf{x}_1, t_2), \dots, \\ &\quad f(\mathbf{x}_{nb}, t_2), f(\mathbf{x}_1, t_m), \dots, f(\mathbf{x}_{nb}, t_m)]^T. \end{aligned} \quad (46)$$

Now, considering Eq. (1), utilizing the collocation nodes and plugging equations (43) and (44) into Eq. (1) lead to the following matrix form:

$$[E]\text{vec}(\mathbf{U}) = \mathbf{F}.$$

In order to compute vector  $\text{vec}(\mathbf{U})$ , the above expression system should be solved to obtain the coefficients. In order to compute vector  $\text{vec}(\mathbf{U})$ , the above expression system should be solved to obtain the coefficients.

#### 4. NUMERICAL EXPERIMENTS

In this section, several examples are implemented to indicate the applicability and effectiveness of the described method for solving two-dimensional time-fractional diffusion equation. Examples are reported to demonstrate influences of the value of order fractional on the numerical results. We present tables and plots of solution for different values of collocation points at various final times. The numerical results vouch for the stability and the accuracy of the proposed computational procedure. It is worthy to note that convergence of the proposed method is not based on certain values of fractional order  $\alpha$ . Thus, we tabulate the numerical results for values of fractional order  $\alpha$  respect to  $N_x$ . The analytical solution of the examples is given as a comparison

with the PD numerical solution. To assess the accuracy of the presented PD method, the relative  $L_2$  norm errors are exploited. The discrete relative  $L_2$  and  $L_\infty$  norms of error are deemed as:

$$\begin{aligned} L_2 &= |u_{\text{exact}}(\mathbf{x}_i, n\tau) - u_{\text{approx}}(\mathbf{x}_i, n\tau)|, \\ L_\infty &= \max_{1 \leq n \leq N} \max_{\mathbf{x}_i \in \Omega} |(u_{\text{exact}}(\mathbf{x}_i, n\tau) \\ &\quad - u_{\text{approx}}(\mathbf{x}_i, n\tau)|, \\ \text{RMS} &= \sqrt{\frac{\sum_{i=1}^N u_{\text{exact}}(\mathbf{x}_i) - u_{\text{approx}}(\mathbf{x}_i)}{N}}, \end{aligned} \quad (47)$$

where  $u_{\text{exact}}$  and  $u_{\text{approx}}$  denote the exact and approximation solutions, respectively. Also, without loss of generality, we consider  $N_x = N_y$  where  $N_x$  and  $N_y$  are the number of nodes in  $x$  and  $y$  direction, respectively.

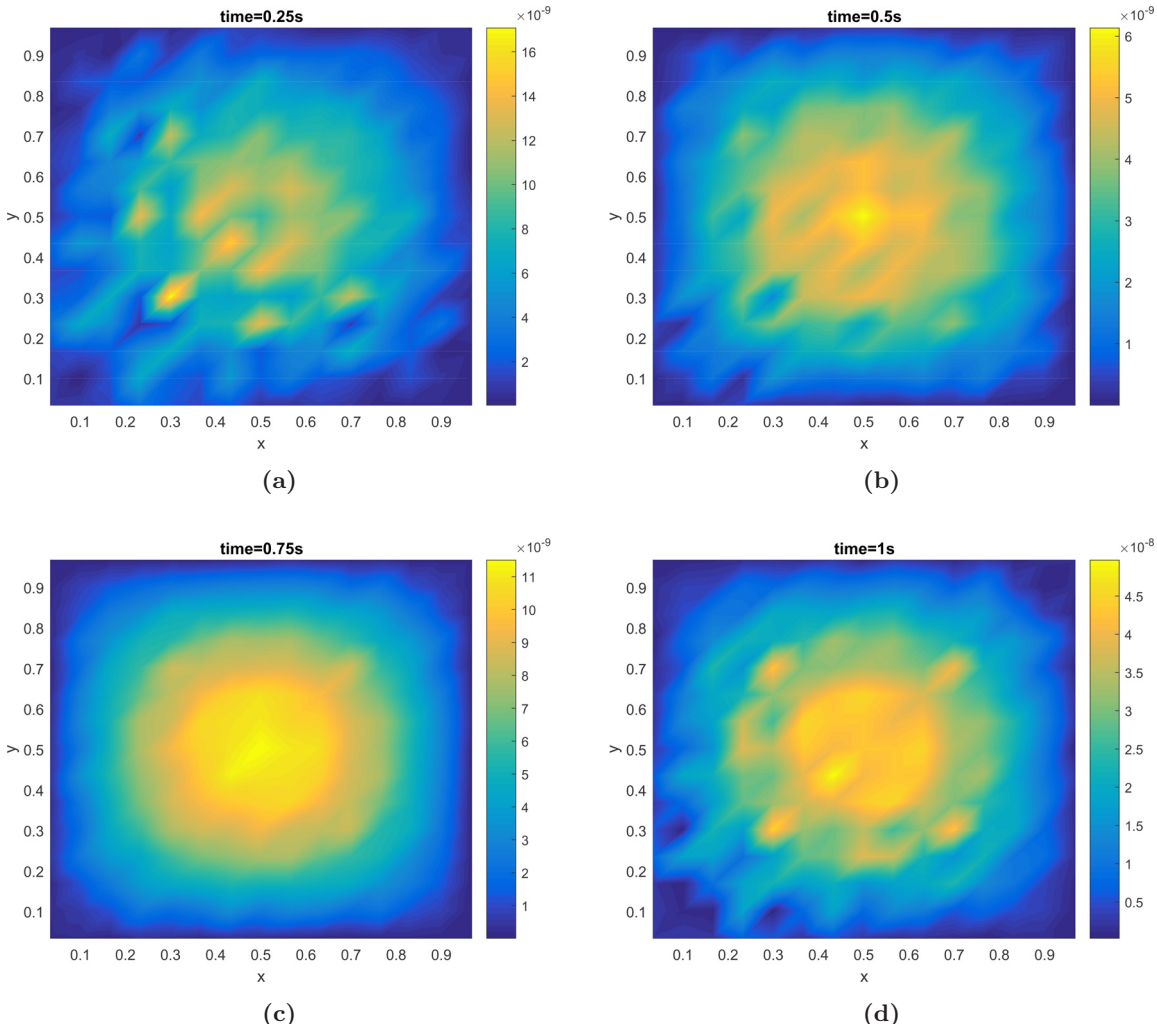
**Example 1.** In this example, we consider two-dimensional time fractional diffusion equation. All the conditions are computable from the analytical solution as follows:

$$u(\mathbf{x}, t) = t^2(x^2 - x)(y^2 - y) \quad (48)$$

and force term can be expressed as  $f(x, y, t) = \frac{2t^{2-\alpha}}{\Gamma(2-\alpha)}(x^2 - x)(y^2 - y) - 2t^2(x^2 - x + y^2 - y)$ , where  $\Omega = [0, 1]^2$  is the computational domain and  $\partial\Omega$  is the boundary of  $\Omega$ . We adopt the proposed PD approach for computing the numerical approximation with various values of  $N_x$ ,  $N_y$ ,  $m$  and  $\alpha$  on the computational domain at final time  $T = 1$ . Table 1 illustrates the convergency, absolute error, in the diverse values of  $N_x$  and  $\alpha$ . These numerical results confirm the convergence of the proposed PD method. As can be seen in Fig. 3, the behaviors of the norm errors associated with computational domain for  $N_x = N_y = 15$  and  $\alpha = 0.5$  in various time levels are shown. Figure 4 demonstrates the PD solutions at different time levels for  $N_x = N_y = 15$  and  $m = 5$  and  $\alpha = 0.5$ . Figure 5 (right-hand) reported RMS error for diverse values of  $\alpha$  at final time  $T = 1$  with  $N_x = N_y = 15$ , and the left-hand side presents the RMS error versus  $N_x$  for various  $m$ ,  $\alpha = 0.9$  at  $T = 1$  in Example 1. Figure 6 reveals the convergence of the method with respect to the degree of Legendre polynomials  $m$ , i.e. ( $m = 3, 4, 5, 6$ ) for different values of  $\alpha$ , i.e. ( $\alpha = 0.3, 0.5, 0.7$ ). The most striking result to emerge from the graphs and table above is that excellent agreements have been observed between numerical outcomes and analytical solution.

**Table 1** Absolute Error for Different  $\alpha$  With Respect to Spatial Points  $N_x$  When  $m = 5$  in Example 1.

| $N_x$ | $\alpha = 0.1$ | $\alpha = 0.3$ | $\alpha = 0.5$ | $\alpha = 0.7$ | $\alpha = 0.9$ |
|-------|----------------|----------------|----------------|----------------|----------------|
| 5     | 1.1970E-06     | 4.9798E-06     | 9.6090E-06     | 1.1683E-05     | 1.5932E-06     |
| 10    | 9.3109E-07     | 9.8446E-07     | 1.9294E-06     | 4.0260E-06     | 2.6301E-06     |
| 15    | 2.6989E-07     | 9.5109E-07     | 1.8817E-06     | 2.2707E-06     | 1.9979E-06     |
| 27    | 2.4256E-07     | 9.4741E-07     | 1.8322E-06     | 2.2322E-06     | 1.8594E-06     |
| 40    | 2.2518E-07     | 9.4730E-07     | 1.7992E-06     | 2.2076E-06     | 1.8159E-06     |


**Fig. 3** Diagrams (a)–(d) are the error functions with  $m = 5$ ,  $\alpha = 0.5$  and  $N_x = N_y = 15$  at different times in Example 1.

**Example 2.** As the latter example, we consider problem (1). The boundary condition and initial condition for the numerical solution are compatible with the analytical solution:

$$u(\mathbf{x}, t) = t^3(x + y)(2 - x - y).$$

We have exploited the presented method with different values of  $N_x$ ,  $m$  and  $\alpha$  on the computational region at final time  $T = 1$ . The numerical results reported in Fig. 7 depict the obtained responses for the absolute errors and contour plots with different time levels. The convergence of the proposed

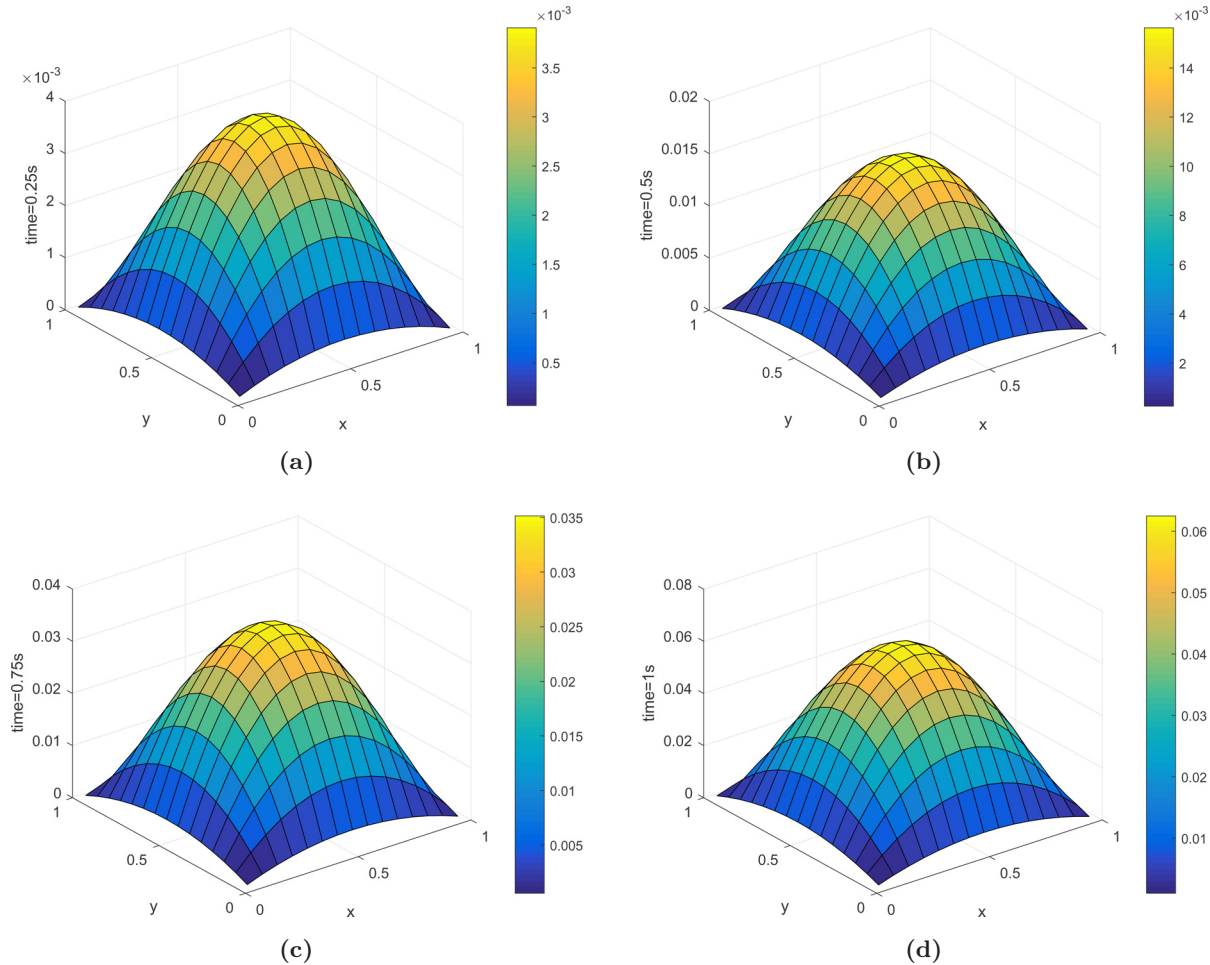


**Fig. 4** Graphs (a)–(d) are the PD method at different times for  $N_x = N_y = 15$ ,  $m = 5$  and  $\alpha = 0.5$  where computational domain  $[0, 1]^2$  in Example 1.

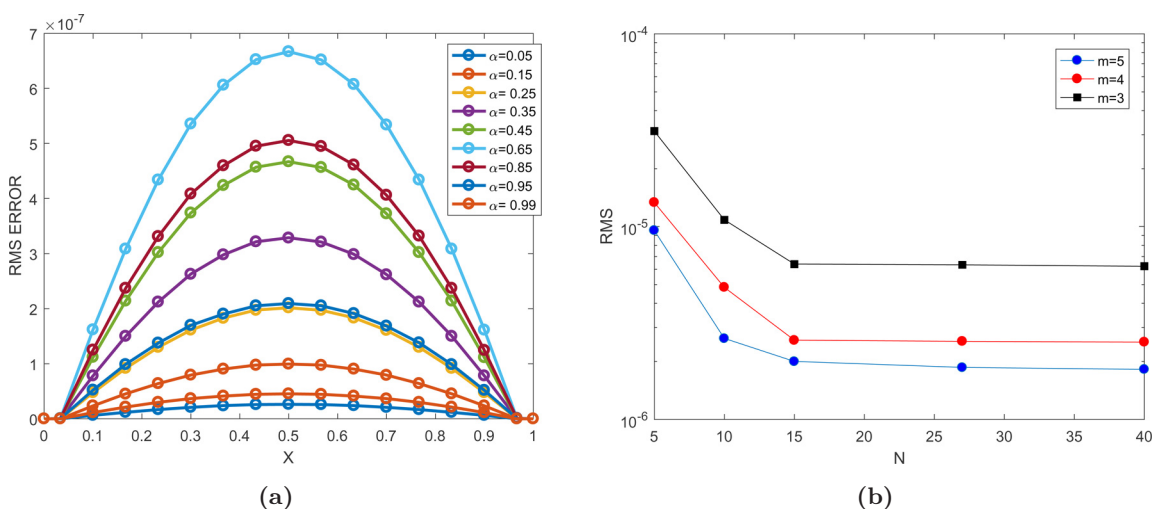


**Fig. 5** The graph (a) is the RMS error for different  $\alpha = 0.5$ ,  $N_x = N_y = 15$  and  $T = 1$ , graph (b) represents the RMS error versus  $N_x$  for different  $m$  and  $\alpha = 0.5$  in Example 1.

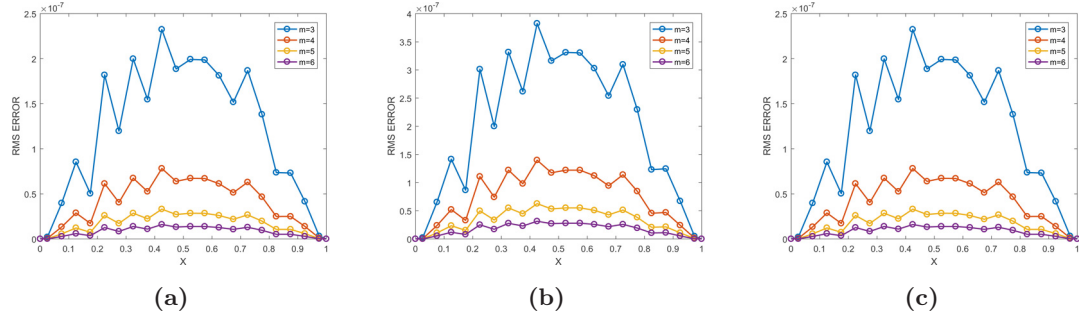


**Fig. 6** Graphs (a)–(c) are the error functions of for  $N_x = N_y = 20$  with  $\alpha = 0.3$  (left),  $\alpha = 0.5$  (middle) and  $\alpha = 0.7$  (right) with different  $m$  in Example 1.

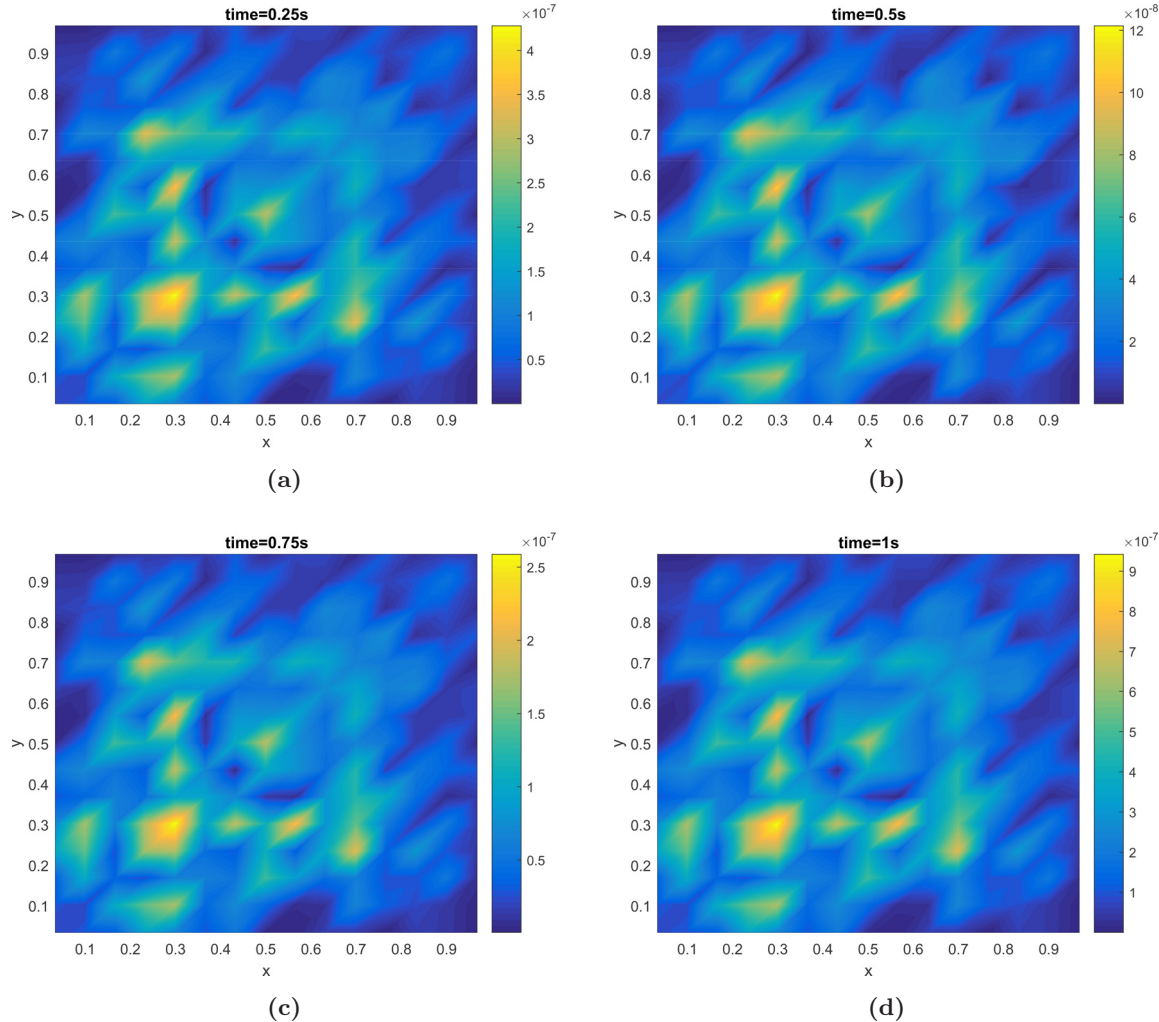


**Fig. 7** Diagrams (a)–(d) are the error functions with  $m = 5$ ,  $\alpha = 0.5$  and  $N_x = N_y = 15$  at different times in Example 2.

PD method is tabulated in Table 2. Table 3 lists two kinds of error,  $L_2$  and  $L_\infty$ , between various values of  $m$  at different times  $t = 0.25, 0.5, 0.75$  and 1 for  $N_x = N_y = 15$  and  $\alpha = 0.3$ . As can be seen in Fig. 7, the manner of the norm errors

is associated with the computational domain for  $N_x = N_y = 20$  and  $\alpha = 0.3$  in different time levels. Figure 8 demonstrates the numerical solutions at different time levels for  $N_x = N_y = 20$  and  $m = 5$  and  $\alpha = 0.3$ . Figure 9 (right-hand) demonstrates

**Table 2** Convergency of the Method With Respect to  $N$  When  $m = 6$  (Absolute Error) for Different  $\alpha$  in Example 2.

| $N_x$ | $\alpha = 0.1$ | $\alpha = 0.3$ | $\alpha = 0.5$ | $\alpha = 0.7$ | $\alpha = 0.9$ |
|-------|----------------|----------------|----------------|----------------|----------------|
| 5     | 5.8442E-6      | 2.4289E-6      | 4.7699E-5      | 6.0754E-5      | 3.7080E-5      |
| 10    | 1.9196E-6      | 7.8980E-6      | 1.5107E-5      | 1.8206E-5      | 1.3248E-5      |
| 15    | 1.2989E-6      | 5.2588E-6      | 1.0179E-5      | 1.4065E-5      | 1.1853E-5      |
| 20    | 6.2741E-7      | 2.6517E-6      | 5.3598E-6      | 7.2342E-6      | 4.8006E-6      |
| 30    | 5.1717E-7      | 2.1011E-6      | 3.9550E-6      | 4.7305E-6      | 4.0119E-6      |

**Table 3** Absolute Error for Different  $m$  in Example 2.

| t              | $m = 4$    |           | $m = 8$    |           | $m = 12$   |           |           |
|----------------|------------|-----------|------------|-----------|------------|-----------|-----------|
|                | $L_\infty$ | $L_2$     | $L_\infty$ | $L_2$     | $L_\infty$ | $L_2$     |           |
| $\alpha = 0.3$ | 0.25       | 5.8442E-6 | 2.4289E-6  | 4.2796E-7 | 1.8485E-6  | 1.0954E-8 | 4.4926E-8 |
|                | 0.5        | 1.9196E-6 | 7.8980E-6  | 1.2140E-7 | 5.3772E-6  | 9.1224E-9 | 4.1992E-8 |
|                | 0.75       | 1.2989E-6 | 2.6517E-6  | 2.5886E-7 | 1.1079E-6  | 1.7456E-8 | 7.7374E-8 |
|                | 1          | 6.2741E-7 | 2.6517E-6  | 9.4200E-7 | 4.0534E-6  | 7.9832E-8 | 3.4440E-7 |

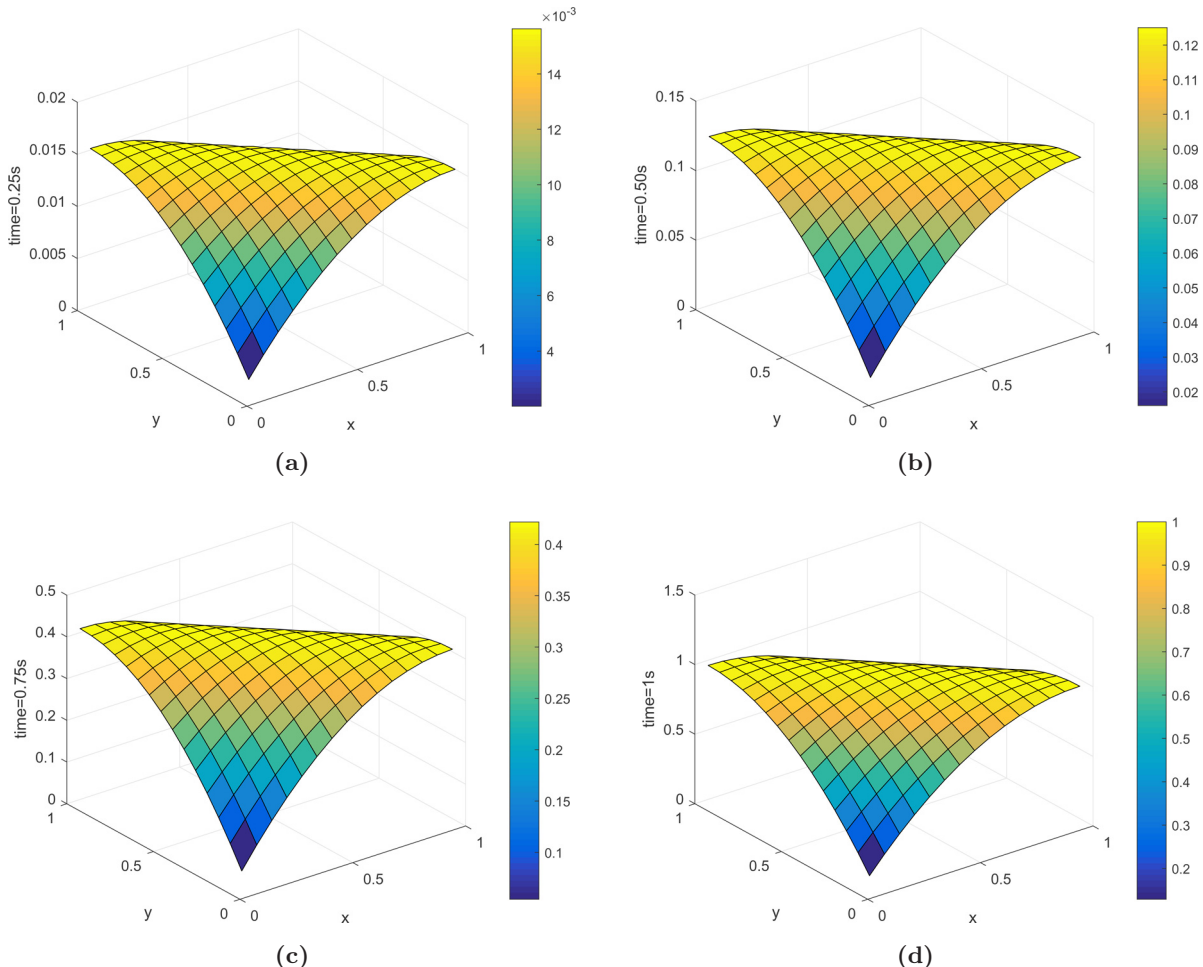


**Fig. 8** Graphs (a)–(d) are the PD method at different times for  $N_x = N_y = 15$ ,  $m = 5$  and  $\alpha = 0.5$  where computational domain  $[0, 1]^2$  in Example 2.

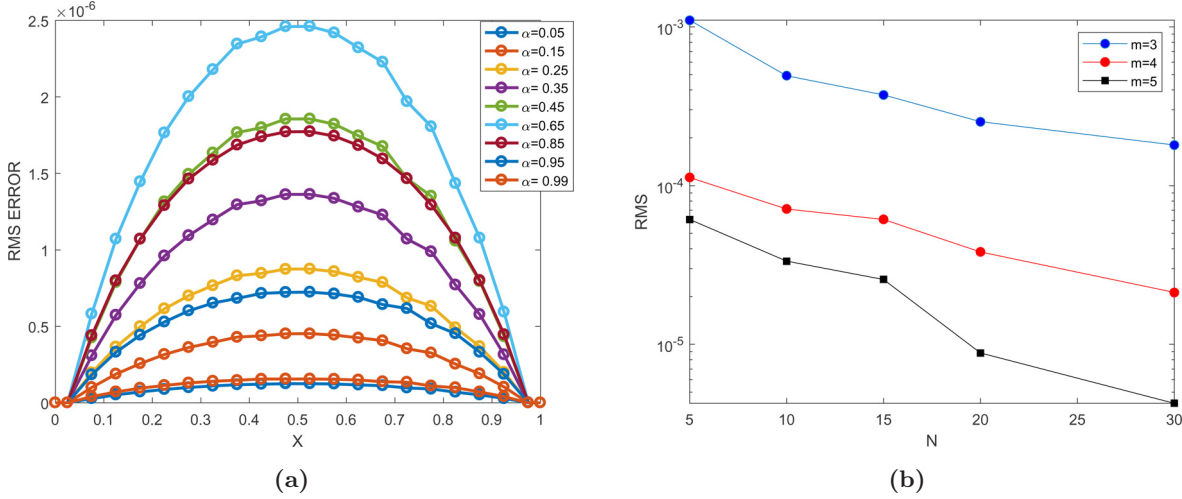


**Fig. 9** The graph (a) is the RMS error for different  $\alpha = 0.5$ ,  $N_x = N_y = 15$  and  $T = 1$ , the graph (b) represent the RMS error versus  $N_x$  for different  $m$  and  $\alpha = 0.5$  in Example 2.

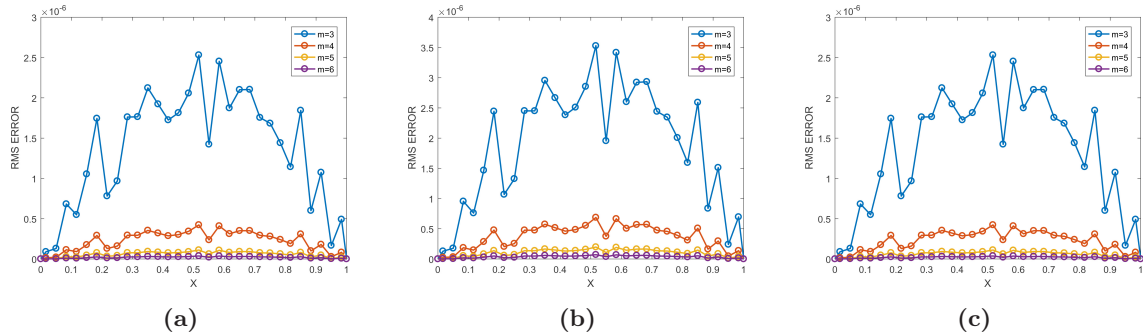


**Fig. 10** The graph (a)–(c) are the error functions of for  $N_x = N_y = 20$  with  $\alpha = 0.3$  (left),  $\alpha = 0.5$  (middle) and  $\alpha = 0.7$  (right) with different  $m$  in Example 2.

the RMS error for diverse values of  $\alpha$  at final time  $T = 1$  with  $N_x = N_y = 15$ , and the left-hand side indicates the RMS error versus  $N_x$  for various  $m$ ,  $\alpha = 0.3$  at  $T = 1$  in Example 2. Figure 10 plots the convergence of the method with respect to degree of Legendre polynomials  $m$ , i.e. ( $m = 3, 4, 5, 6$ ) for different values of  $\alpha$ , i.e. ( $\alpha = 0.3, 0.5, 0.7$ ). It is apparent from tables and figures the excellent agreement between presented method and analytical solution which reveals the reliability of the PD scheme.

**Example 3.** As the third example, we consider the following fractional parabolic equation with initial and boundary conditions:

$$\begin{cases} {}_0^c D_t^\alpha u(\mathbf{x}, t) = \Delta u(\mathbf{x}, t) - \gamma u(\mathbf{x}, t) + f(\mathbf{x}, t), \\ \quad (x, y) \in Q, \quad 0 < t \leq T, \\ u(\mathbf{x}, t) = \rho(\mathbf{x}, t), \quad (x, y) \in \Omega, \\ u(\mathbf{x}, 0) = u_0(\mathbf{x}), \quad (x, y) \in \partial\Omega, \quad 0 < t \leq T, \end{cases} \quad (49)$$

We choose a suitable right-hand side function  $f$  such that the exact solution of Eq. (49) is  $u = t^4 \sin(x) \sin(y)$ . The initial and boundary conditions can be determined according to exact solution. Figure 11 depicts obtained responses for the absolute errors and contour plots with different time levels. Next, we investigate the effect of the domain on the maximum errors. The convergence of the proposed PD technics is elucidated in Table 4. As can be seen in Fig. 12, the numerical solutions are demonstrated at various time steps for  $N_x = N_y = 20$  and  $m = 5$  and  $\alpha = 0.3$ . The RMS error for different values of  $\alpha$  is yielded from the proposed method and is reported in Figs. 13 and 14. They show the convergency of the method with respect to  $m$  and  $N_x$ , and also demonstrate the RMS error for some values of  $\alpha$ .

**Example 4.** As the last test problem, we consider the two-dimensional time fractional diffusion equation. The analytical solution can be expressed as

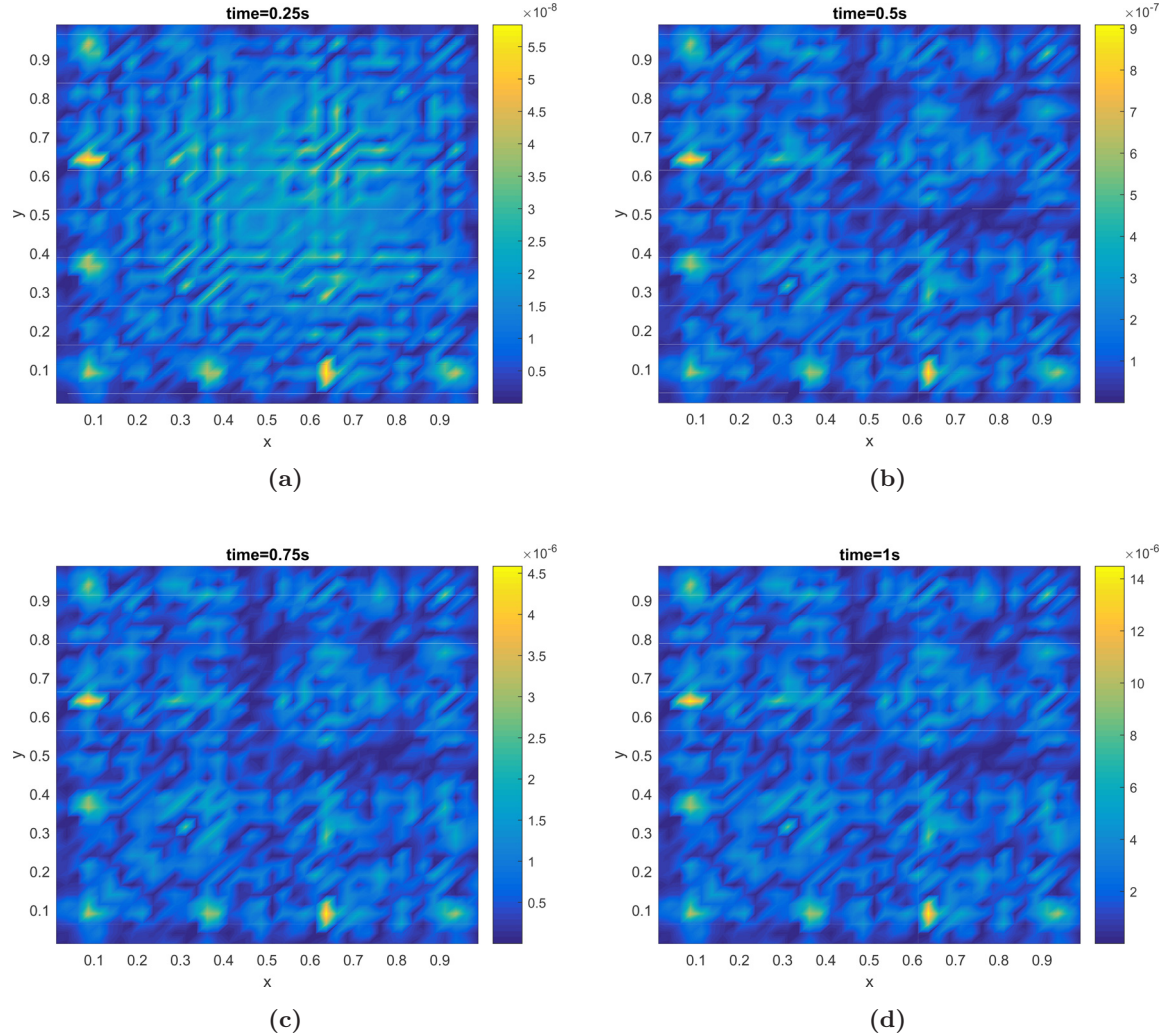


**Fig. 11** The diagram (a)–(d) are the error functions with  $m = 5$ ,  $\alpha = 0.5$  and  $N_x = N_y = 15$  at different time in Example 3.

**Table 4** Illustrates the Convergency of the Method With Respect to  $N_x$  When  $m = 6$  (Absolute Error) for Different  $\alpha$  in Example 3.

| $N_x$ | $\alpha = 0.1$ | $\alpha = 0.3$ | $\alpha = 0.5$ | $\alpha = 0.7$ | $\alpha = 0.9$ |
|-------|----------------|----------------|----------------|----------------|----------------|
| 10    | 0.0218         | 0.0220         | 0.0222         | 0.0225         | 0.0229         |
| 15    | 9.9645E-4      | 9.8640E-4      | 9.7503E-4      | 9.6263E-4      | 9.4949E-4      |
| 25    | 8.9202E-4      | 8.8368E-4      | 8.3066E-4      | 7.9229E-4      | 7.4882E-4      |
| 35    | 4.7643E-5      | 4.7920E-5      | 4.8263E-5      | 4.8521E-5      | 4.8379E-5      |
| 40    | 1.4435E-5      | 1.4468E-5      | 1.4512E-5      | 1.4561E-5      | 1.4590E-5      |

$t^5 \exp(x + y)$ , the initial value is given by

$$\begin{cases} u(\mathbf{x}, 0) = \exp(x + y), & \mathbf{x} \in \Omega, \\ u(\mathbf{x}, t) = t^5 \exp(x + y), & (x, y) \in \partial\Omega, \quad 0 < t \leq T, \end{cases}$$

the proposed approach is fulfilled to investigate the fractional diffusion problem. To seek the effect of the degree of Legendre polynomials at different

time levels, the numerical results with respect to  $m = 4, 8, 12$  are listed in Table 5. Figure 15 depicts RMS error for different  $\sigma = 0.5$  and the numerical solution. Figure 16a is devoted to assess the treatment of the RMS error associated with  $T = 1$ . Figure 16b represents the numerical solution of PD method for  $N_x = 40$ ,  $m = 10$ , and  $\alpha = 0.7$ .

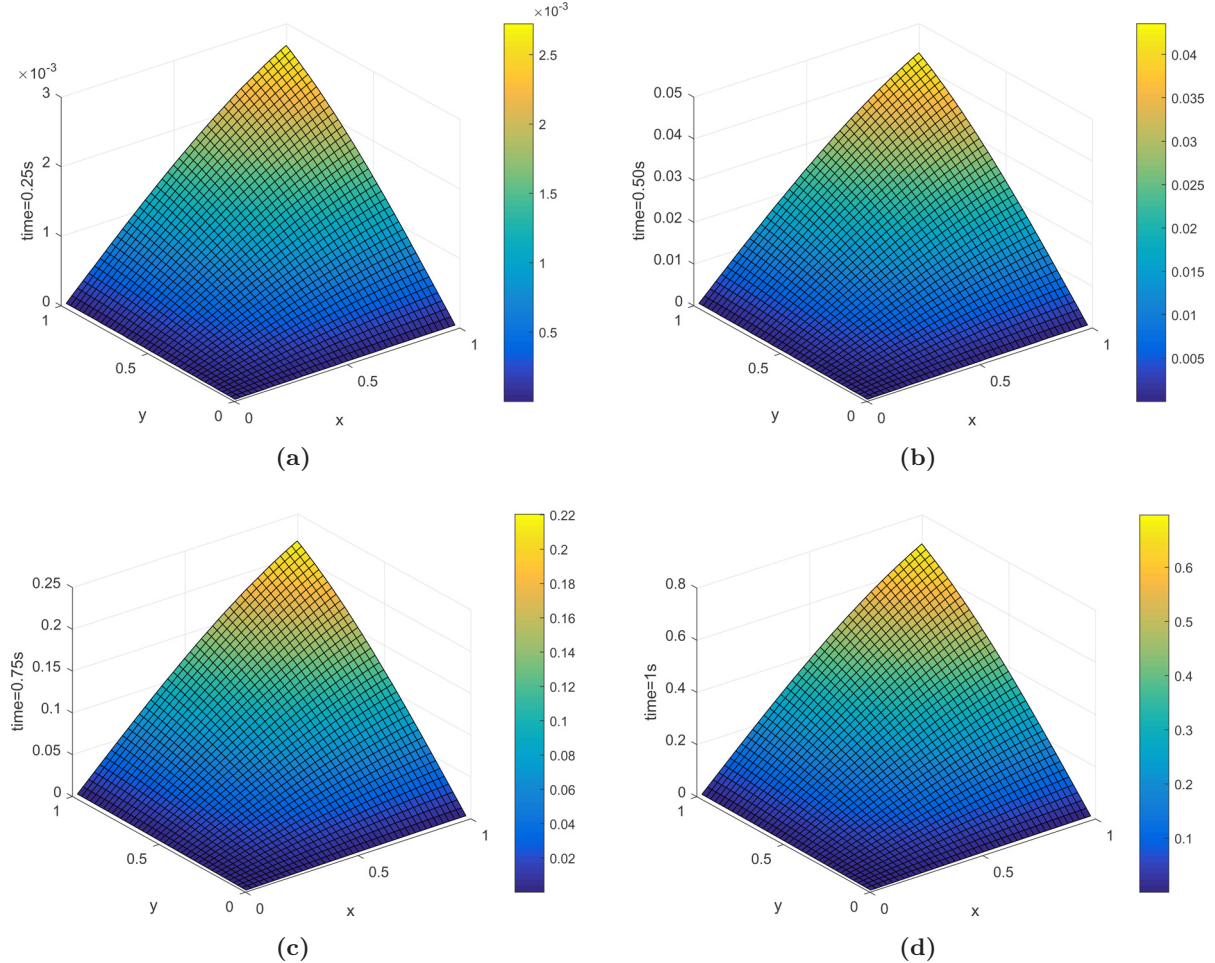


**Fig. 12** The graph (a)–(d) are the PD method at different time for  $N_x = N_y = 15$ ,  $m = 5$  and  $\alpha = 0.5$  where computational domain  $[0, 1]^2$  in Example 3.

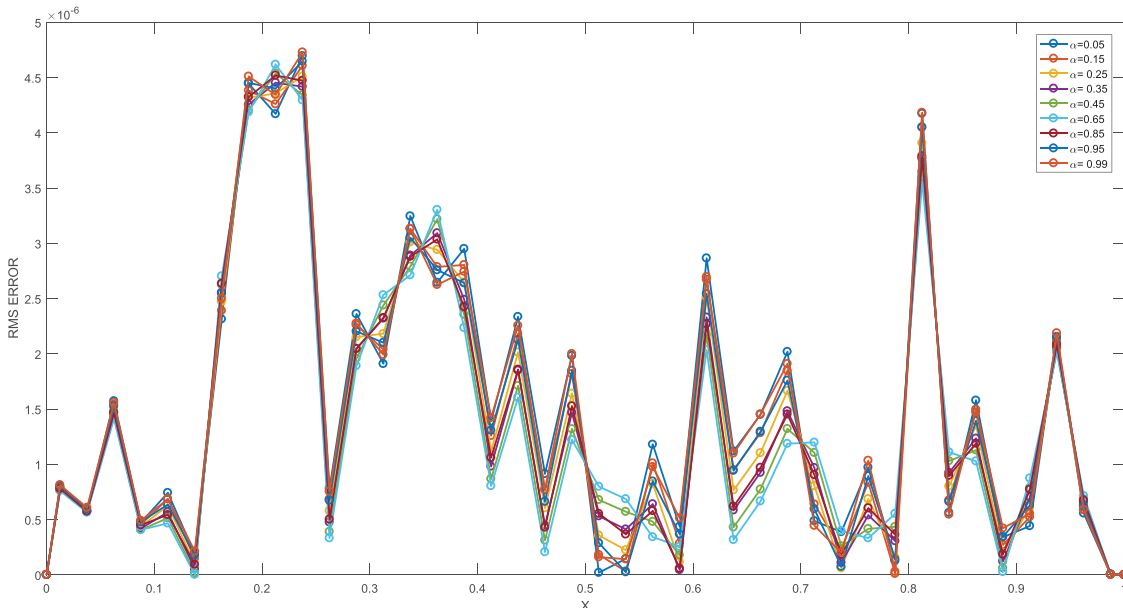


**Fig. 13** The graph is the RMS error for different  $\alpha$  and  $N_x = N_y = 15$  at  $T = 1$  in Example 3.

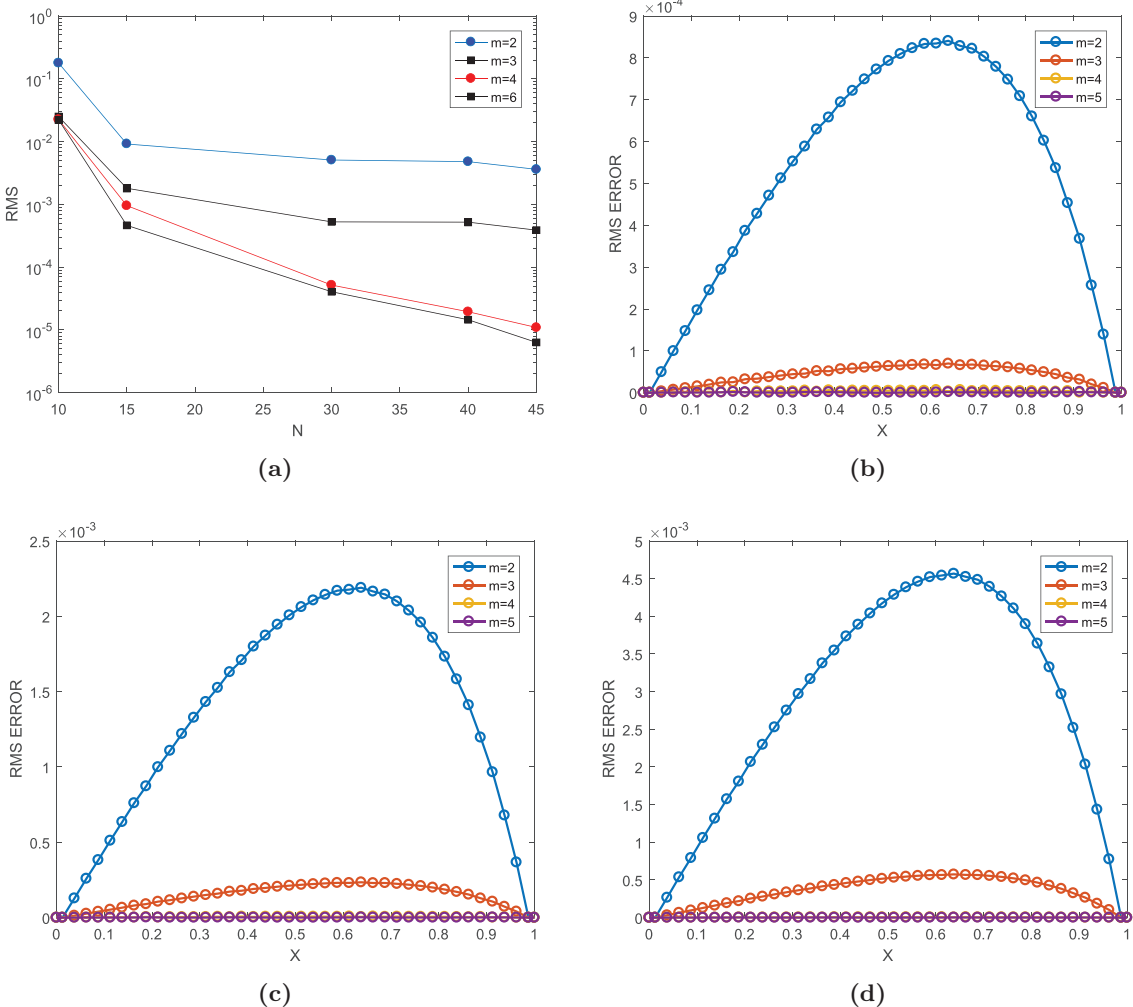


**Fig. 14** The graph (a) is the PD method at different time  $m = 2, 3, 4, 5, 6$  for  $N_x = N_y = 15$  and  $\alpha = 0.7$  when computational domain is  $[0, 1]^2$  and (b)–(d) demonstrate the result of study with respect to  $\alpha = 0.3, 0.5$  and  $0.7$  in Example 3.

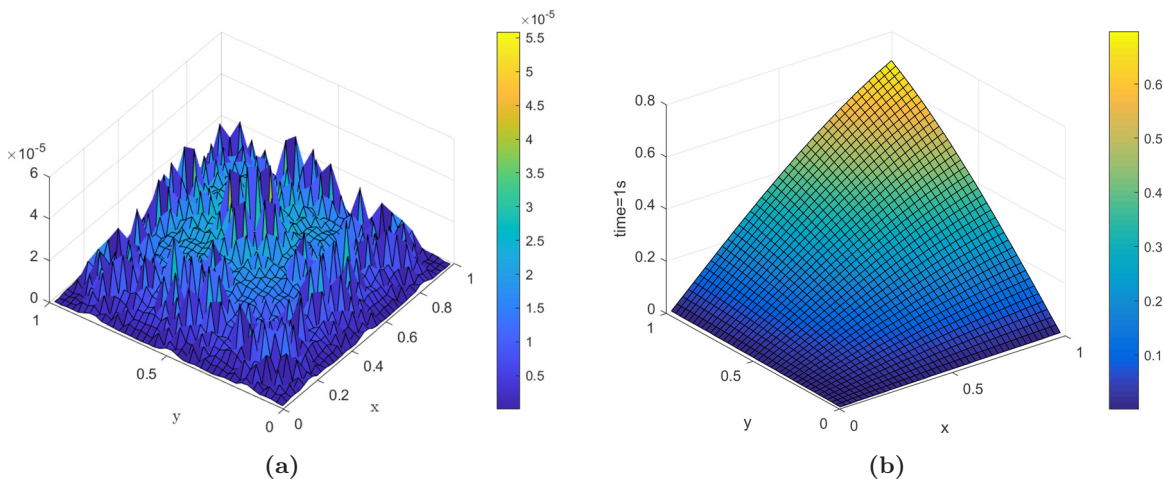


**Fig. 15** The graph (a) is the RMS error for different  $\alpha = 0.5$  at the graph (b) represent the numerical solution versus  $N_x = 40$  for different  $m$ ,  $\alpha = 0.5$  in Example 4.

**Table 5** Absolute Error for Different Time Level in Example 4.

| T              | $m = 4$    |           | $m = 8$    |           | $m = 12$   |           |           |
|----------------|------------|-----------|------------|-----------|------------|-----------|-----------|
|                | $L_\infty$ | $L_2$     | $L_\infty$ | $L_2$     | $L_\infty$ | $L_2$     |           |
| $\alpha = 0.5$ | 0.25       | 0.0010    | 0.0209     | 9.0391E-8 | 1.5010E-6  | 2.940E-8  | 3.0540E-7 |
|                | 0.5        | 3.9523E-4 | 0.0075     | 9.0880E-6 | 9.6228E-6  | 9.0641E-6 | 9.6157E-5 |
|                | 0.75       | 8.9935E-4 | 0.0170     | 6.9488E-6 | 7.3243E-6  | 9.6229E-6 | 7.3110E-5 |
|                | 1          | 1.5000E-3 | 2.2900E-3  | 2.9290E-5 | 3.0805E-4  | 2.9110E-5 | 3.0767E-4 |

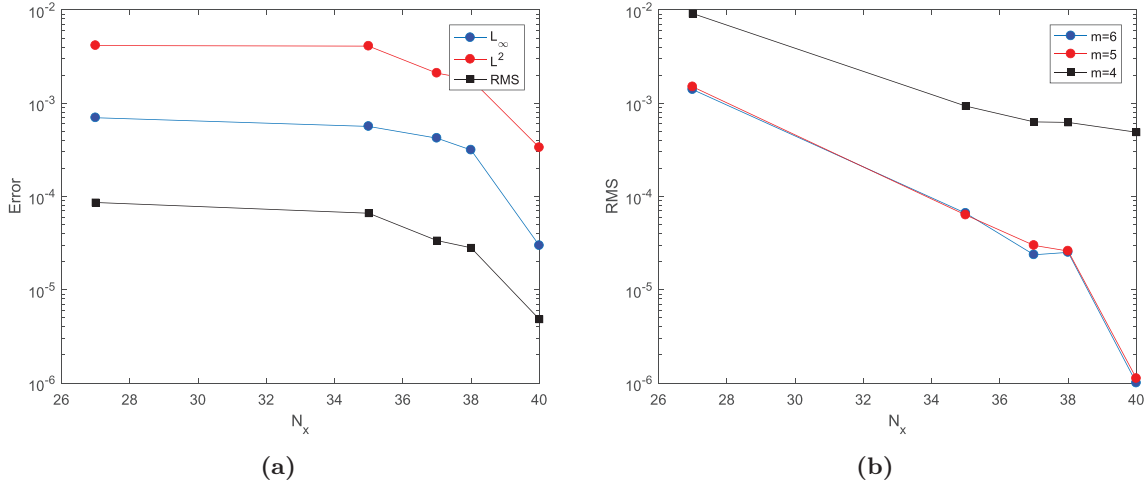


**Fig. 16** The graph (a) is the RMS error for different  $\alpha = 0.5$  at the graph (b) represent the numerical exact solution error versus  $N_x = 40$  for different  $m$   $\alpha = 0.5$  in Example 4.

## 5. CONCLUSION

Throughout this study, the non-local approach developed a robust novel method for computing 2D time-fractional diffusion equation. The PDDO for spatial domain and Legendre orthogonal polynomials to generate the Lagrange multiplier method for discretizing time fractional term has been exploited. Hence, the intended problem reduced into a system of algebraic equation. The proposal meshless method is one of the effective techniques in handling without using background integration cells. Several numerical examples were utilized to indicate the validity and the reliability of the proposed method. For all such examples, numerical convergence and stability of error have been investigated.

## ACKNOWLEDGMENTS

This work is supported by the National Natural Science Foundation of China (No. 12172159), National Natural Science Foundation of Jiangxi Provence (No. 2021BAB211022). The authors are very thankful for Jiangxi double thousand talents support (No. jxsq2018106027).

## REFERENCES

1. A. Altan, S. Karasu and E. Zio, A new hybrid model for wind speed forecasting combining long short-term memory neural network, decomposition methods and grey wolf optimizer, *Appl. Soft Comput.* **100** (2021) 106996.
2. V. R. Hosseini, M. Remazani, W. Zou and S. Banishashemii, Stochastic model for multi-term time-fractional diffusion equations with noise, *Thermal Sci.* **25**(2) (2021) 287–293.
3. S. Karasu, A. Altan, S. Bekiros and W. Ahmad, A new forecasting model with wrapper-based feature selection approach using multi-objective optimization technique for chaotic crude oil time series, *Energy* **212** (2020) 118750.
4. P. P. Mehta, T. Zaki, C. Meneveau and G. Karniadakis, Fractional Reynolds-averaged Navier–Stokes equations (f-RANS) for modeling of transitional and turbulent boundary layers, in *APS Division of Fluid Dynamics Meeting Abstracts* (2020), <https://ui.adsabs.harvard.edu/abs/2020APS.DFD-X11001P>.
5. F. Song, G. Pange, C. Meneveau and G. Karniadakis, Fractional physical-inform neural networks (fPINNs) for turbulent flows, in *APS Division*

- of Fluid Dynamics Meeting Abstracts (2019), <https://ui.adsabs.harvard.edu/abs/2019APS.DFD-A19002S>.
6. V. R. Hosseini, E. Shivanian and W. Chen, Local radial point interpolation (MLRPI) method for solving time fractional diffusion-wave equation with damping, *J. Comput. Phys.* **312** (2016) 307–332.
  7. P. P. Mehta, G. Pang, F. Song and G. E. Karniadakis, Discovering a universal variable-order fractional model for turbulent Couette flow using a physics-informed neural network, *Fractional Calc. Appl. Anal.* **22**(6) (2019) 1675–1688.
  8. S. Rashid, S. Sultana, Y. Karaca, A. Khalid and Y.-M. Chu, Some further extensions considering discrete proportional fractional operators, *Fractals* **30** (2021) 2240026.
  9. M. Al-Qurashi, S. Rashid, Y. Karaca, Z. Hammouch, D. Baleanu and Y.-M. Chu, Achieving more precise bounds based on double and triple integral as proposed by generalized proportional fractional operators in the Hilfer sense, *Fractals* **29**(5) (2021) 2140027–2140066.
  10. X. Li and C. Xu, A space-time spectral method for the time fractional diffusion equation, *SIAM J. Numer. Anal.* **47**(3) (2009) 2108–2131.
  11. F. Mainardi, G. Pagnini and R. Gorenflo, Some aspects of fractional diffusion equations of single and distributed order, *Appl. Math. Comput.* **187**(1) (2007) 295–305.
  12. D. Baleanu, M. Hassan Abadi, A. Jajarmi, K. Zarghami Vahid and J. J. Nieto, A new comparative study on the general fractional model of COVID-19 with isolation and quarantine effects, *Alex. Eng. J.* **61**(6) (2022) 4779–4791.
  13. V. S. Erturk, E. Godwe, D. Baleanu, P. Kumar, J. Asad and A. Jajarmi, Novel fractional-order Lagrangian to describe motion of beam on nanowire, *Acta Phys. Polon. A* **140**(3) (2021) 265.
  14. N. Iqbal and Y. Karaca, Complex Fractional-order HIV diffusion model based on amplitude equations with turing patterns and turing instability, *Fractals* **29** (2021) 2140013.
  15. A. Jajarmi, D. Baleanu, K. Z. Vahid, H. M. Pirouz and J. H. Asad, A new and general fractional Lagrangian approach: A capacitor microphone case study, *Results Phys.* **31** (2021) 104950.
  16. A. Jajarmi, D. Baleanu, K. Z. Vahid and S. Mobayen, A general fractional formulation and tracking control for immunogenic tumor dynamics, *Math. Methods Appl. Sci.* **45** (2021) 667–680.
  17. M. Shadabfar and L. Cheng, Probabilistic approach for optimal portfolio selection using a hybrid Monte Carlo simulation and Markowitz model, *Alex. Eng. J.* **59**(5) (2020) 3381–3393.
  18. M.-K. Wang, S. Rashid, Y. Karaca, D. Baleanu and Y.-M. Chu, New multi-functional approach for  $\kappa$ th-order differentiability governed by fractional calculus via approximately generalized  $(\psi, \cdot)$ -convex functions in hilbert space, *Fractals* **29**(5) (2021) 2140019–2140769.
  19. Z. Li, D. Huang, Y. Xu and K. Yan, Nonlocal steady-state thermoelastic analysis of functionally graded materials by using peridynamic differential operator, *Appl. Math. Model.* **93** (2021) 294–313.
  20. M. Behzadinasab and J. T. Foster, A semi-Lagrangian constitutive correspondence framework for peridynamics, *J. Mech. Phys. Solids* **137** (2020) 103862.
  21. Y. H. Bie, X. Y. Cui and Z. C. Li, A coupling approach of state-based peridynamics with node-based smoothed finite element method, *Comput. Methods Appl. Mech. Eng.* **331** (2018) 675–700.
  22. X. Gu, E. Madenci and Q. Zhang, Revisit of non-ordinary state-based peridynamics, *Eng. Fracture Mech.* **190** (2018) 31–52.
  23. T. Rabczuk and H. Ren, A peridynamics formulation for quasi-static fracture and contact in rock, *Eng. Geol.* **225** (2017) 42–48.
  24. A. Shojaei, U. Galvanetto, T. Rabczuk, A. Jenabi and M. Zaccariotto, A generalized finite difference method based on the Peridynamic differential operator for the solution of problems in bounded and unbounded domains, *Comput. Methods Appl. Mech. Eng.* **343** (2019) 100–126.
  25. S. Bazazzadeh, A. Shojaei, M. Zaccariotto and U. Galvanetto, Application of the peridynamic differential operator to the solution of sloshing problems in tanks, *Eng. Comput.* **36**(1) (2018) 45–83.
  26. S. Bazazzadeh, M. Zaccariotto and U. Galvanetto, Fatigue degradation strategies to simulate crack propagation using peridynamic based computational methods, *Latin Am. J. Solids Struct.* **16**(2) (2019), <https://doi.org/10.1590/1679-78255022>.
  27. B. Chu, Q. Liu, L. Liu, X. Lai and H. Mei, A rate-dependent peridynamic model for the dynamic behavior of ceramic materials, *Comput. Model. Eng. Sci.* **124**(1) (2020) 151–178.
  28. H. Jafari, B. Mehdinejadiani and D. Baleanu, Fractional calculus for modeling unconfined groundwater, *Applications in Engineering, Life and Social Sciences*, Vol. 119 (De Gruyter, 2019).
  29. A. S. Khoojine, M. Mahsuli, M. Shadabfar, V. R. Hosseini and H. Kordestani, A proposed fractional dynamic system and Monte Carlo-based back analysis for simulating the spreading profile of COVID-19, *Euro. Phys. J. Spec. Top.* **2022** (2022) 1–11.
  30. E. Madenci, A. Barut and M. Futch, Peridynamic differential operator and its applications, *Comput. Methods Appl. Mech. Eng.* **304** (2016) 408–451.
  31. V. R. Hosseini and W. Zou, The peridynamic differential operator for solving time-fractional partial

- differential equations, *Nonlinear Dynam.* (2022) 1–28, <https://doi.org/10.1007/s11071-022-07424-4>.
32. M. D'Elia and M. Gunzburger, The fractional Laplacian operator on bounded domains as a special case of the nonlocal diffusion operator, *Comput. Math. Appl.* **66**(7) (2013) 1245–1260.
  33. G. Pang, M. D'Elia, M. Parks and G. E. Karniadakis, nPINNs: Nonlocal physics-informed neural networks for a parametrized nonlocal universal Laplacian operator. Algorithms and Applications, *J. Comput. Phys.* **422** (2020) 109760.
  34. M. D'Elia, M. Gulian, H. Olson and G. E. Karniadakis, A unified theory of fractional, non-local, and weighted nonlocal vector calculus, arXiv:2005.07686.
  35. P. C. Di Leoni, T. A Zaki, G. Karniadakis and C. Meneveau, Two-point stress–strain-rate correlation structure and non-local eddy viscosity in turbulent flows, *J. Fluid Mech.* **914** (2021) A6.
  36. Y. Gao and S. Oterkus, Fluid-elastic structure interaction simulation by using ordinary state-based peridynamics and peridynamic differential operator, *Eng. Anal. Bound. Elements* **121** (2020) 126–142.
  37. Y. Gao and S. Oterkus, Multi-phase fluid flow simulation by using peridynamic differential operator, *Ocean Eng.* **216** (2020) 108081.
  38. C. T. Nguyen, S. Oterkus and E. Oterkus, A physics-guided machine learning model for two-dimensional structures based on ordinary state-based peridynamics, *Theor. Appl. Fracture Mech.* **112** (2021) 102872.
  39. C. Atkinson and A. Osseiran, Rational solutions for the time-fractional diffusion equation, *SIAM J. Appl. Math.* **71**(1) (2011) 92–106.
  40. Z.-J. Fu, W. Chen and H.-T. Yang, Boundary particle method for Laplace transformed time fractional diffusion equations, *J. Comput. Phys.* **235** (2013) 52–66.
  41. V. R. Hosseini, F. Yousefi and W.-N. Zou, The numerical solution of high dimensional variable-order time fractional diffusion equation via the singular boundary method, *J. Adv. Res.* **32** (2021) 73–84.
  42. Y. Lin and C. Xu, Finite difference/spectral approximations for the time-fractional diffusion equation, *J. Comput. Phys.* **225**(2) (2007) 1533–1552.
  43. M. Cui, Compact finite difference method for the fractional diffusion equation, *J. Comput. Phys.* **228**(20) (2009) 7792–7804.
  44. V. R. Hosseini, M. Koushki and W. N. Zou, The meshless approach for solving 2D variable-order time-fractional advectiondiffusion equation arising in anomalous transport, *Eng. Comput.* (2021), <https://doi.org/10.1007/s00366-021-01379-7>
  45. A. A. Alikhanov, A new difference scheme for the time fractional diffusion equation, *J. Comput. Phys.* **280** (2015) 424–438.
  46. M. Stynes, E. O'Riordan and J. L. Gracia, Error analysis of a finite difference method on graded meshes for a time-fractional diffusion equation, *SIAM J. Numer. Anal.* **55**(2) (2017) 1057–1079.
  47. A. Lotfi, M. Dehghan and S. A. Yousefi, A numerical technique for solving fractional optimal control problems, *Comput. Math. Appl.* **62**(3) (2011) 1055–1067.
  48. S. A. Silling, Reformulation of elasticity theory for discontinuities and long-range forces, *J. Mech. Phys. Solids* **48**(1) (2000) 175–209.
  49. A. C. Bekar and E. Madenci, Peridynamics enabled learning partial differential equations, *J. Comput. Phys.* **434** (2021) 110193.
  50. E. Madenci, A. Barut and M. Dorduncu, *Peridynamic Differential Operator for Numerical Analysis* (Springer, 2019).
  51. E. Madenci and E. Oterkus, Peridynamic theory, *Peridynamic Theory and Its Applications* (Springer, 2014), pp. 19–43.
  52. E. Kreyszig, *Introductory Functional Analysis with Applications*, Vol. 1 (Wiley, New York, 1978).